LA-13432-SR
Status Report

UC-2000 and UC-940
Issued: March 1998

Status of the WAND (Waste Assay for Nonradioactive Disposal) Project as of July 1997

G. J. Arnone
L. A. Foster
C. L. Foxx
R. C. Hagan
E. R. Martin
S. C. Myers
J. L. Parker

Los Alamos
NATIONAL LABORATORY
Los Alamos, New Mexico 87545

DISCLAIMER

CONTENTS

STATUS OF THE WAND (WASTE ASSAY FOR NONRADIOACTIVE DISPOSAL) PROJECT AS OF JULY 1997

by

G. J. Arnone, L. A. Foster, C. L. Foxx, R. C. Hagan,
E. R. Martin, S. C. Myers, and J. L. Parker

ABSTRACT

The WAND (Waste Assay for Nonradioactive Disposal) system can scan thought-to-be-clean, low-density waste (mostly paper and plastics) to determine whether the levels of any contaminant radioactivity are low enough to justify their disposal in normal public landfills or similar facilities. Such a screening would allow probably at least half of the large volume of low-density waste now buried at high cost in LANL's Rad Waste Landfill (Area G at Technical Area 54 [TA-54]) to be disposed of elsewhere at a much lower cost.

The WAND System consists of a well-shielded bank of six 5-in.-diam phoswich scintillation detectors; a mechanical conveyor system that carries a 12-in.-wide layer of either shredded material or packets of paper sheets beneath the bank of detectors; the electronics needed to process the outputs of the detectors; and a small computer to control the whole system and to perform the data analysis.

WAND system minimum detectable activities (MDAs) for point sources range from ~20 dps for ^{241}Am to approximately 10 times that value for ^{239}Pu, with most other nuclides of interest being between those values, depending upon the emission probabilities of the radiations emitted (usually gamma rays and/or x-rays). The system can also detect beta particles that have energies ≥100 keV, but it is not easy to define an MDA based on beta radiation detection because of the greater absorption of beta particles relative to photons in low Z-materials. The only radioactive nuclides not detectable by the WAND system are pure alpha emitters and very-low-energy beta emitters.

At this time, operating procedures and quality assurance procedures are in place and training materials are available to operators. The system is ready to perform useful work; however, it would be both possible and desirable to upgrade the electronic components and the analysis algorithms.

I. INTRODUCTION

A large volume of clean (radioactive-contaminant-free), low-density waste—mostly paper and plastics—must be buried as possibly radioactive waste at Los Alamos National Laboratory's (LANL's) Rad Waste Landfill (Area G at Technical Area-54 [TA-54]). This is because there is no adequately sensitive process for verifying that the waste is clean enough for safe disposal in the Los Alamos County Landfill or a similar facility. For example, in fiscal year (FY) 1995 the Los Alamos Plutonium Facility disposed of 124 m^3 of this type of waste at Area G, though 50% to 90% of it is estimated to be free of radioactive contamination. For LANL as a whole in 1994, about 500 m^3 of such waste was buried at Area G at a cost of about $1,576 per cubic meter. We estimate that at least 50% of that waste was actually clean. The disposal of this type of waste is an expensive, major problem across the U.S. Department of Energy (DOE) complex. Clearly, if the clean portion of such waste could be verified clean with sufficient sensitivity disposing of it at the Los Alamos County Landfill, or a similar facility, could be justified. Such disposal would cost only about $10 per cubic meter ($40 per metric ton). Thus, even with the additional cost of the verification procedure, a significant savings could be achieved, and the resulting additional capacity at Area G could be saved for waste that is truly radioactive. Recent DOE orders requiring that only radioactive waste be buried at Area G and new requirements that LANL reduce its waste by 50% by the year 1998 have provided further motivation for developing a sensitive verification process.

From 1971 to 1973, a team of researchers in what is now called the Safeguards, Science and Technology Group (NIS-5) investigated the technical problem associated with scanning suspect waste and determining whether contamination levels are below permitted limits. They found that the low-energy L x-rays emitted by high-Z alpha emitters could be used to screen low-density, low-Z waste for the contamination limits permitted at that time. Consequently, they designed and produced a number of instruments based on the use of a single sodium iodide (NaI) scintillation detector that detected low-energy x-rays simultaneously with higher-energy gamma radiation. There was no need to swipe materials. Although the technique was limited to low-density materials, they found that this constitutes the majority of the suspect materials. Because of the lack of funding support in the early 1970s and because it was cheaper at that time to simply dispose of all the unsegregated waste in the low-level dump, the project was dropped in 1973.

In 1993, the original core members of the Waste Assay for Nonradioactive Disposal (WAND) team proposed a waste minimization concept to LANL's Pollution Prevention Program Office (P3O) and to the Albuquerque area office of the DOE. They proposed placing collection containers in all LANL Radioactive Materials Management Areas; these would only be for waste that is quite confidently believed to be nonradioactive. That waste would then be taken to a central location and screened to verify that it is free of radioactive contamination to levels well below the level that available commercial instruments are able to verify. With its extensive collective experience in the nondestructive measurement of special

nuclear materials, the WAND team was to design and build the new verification instrument using the most modern detectors and equipment available. Two team members, who had been involved in Nuclear Technology and Engineering (N-1) development work from 1971 to 1973, had already given much informal thought to improving the original detector configurations to achieve sensitivities that would meet the current much more stringent contamination limits.

This project has used innovative detection hardware and analysis methods, which are briefly explained here, with detailed descriptions provided in later sections of this report.

Because waste from LANL's Plutonium Facility is a major component of the Green is Clean Program, it is important to have equipment that is highly sensitive to alpha-particle-emitting nuclides (plutonium, americium, and uranium contribute the most important of such nuclides). Alpha particles are easily detectable but cannot penetrate a single sheet of paper. From the beginning, the WAND team members decided that screening both sides of every sheet of paper with standard alpha-detecting equipment was intolerably cumbersome and expensive. As mentioned above, all of the alpha-emitting, high-Z nuclides also emit L x-rays (in the 10-keV to 25-keV energy range) that can be used as a basis for detection. Though the L x-rays are emitted in only a fraction of the alpha decays (5% to 35%, depending on the nuclide), they penetrate low-density materials much better than do alpha particles—up to ~25 sheets of paper with only perhaps a 25%-loss from the bottom layer. Because the L x–rays are very low (~15 keV) in the energy range of gamma rays and x-rays emitted by nuclides that might be encountered, the proper detector must be selected if it is to detect radiations over the whole potential range of ~2000 keV. For most standard types of detectors whose volumes are large enough to have the desired high-energy efficiency, low-energy background rates tend to be high (a serious difficulty when one is trying to screen with a high degree of sensitivity). When doing multichannel analyses of detector outputs over a 2000-keV range, one usually wants more channels per thousand electron volts in the important low-energy regions than can easily be achieved over that range. The phoswich-type detector, which was already being used to measure lung burdens of plutonium and uranium, offered the proper blend of properties (see Section III-A-1 of this report for details). The adoption of the phoswich detector was essential to achieving the performance level of the WAND system.

The WAND team also recognized the need to develop a new set of physical standards that would help to prove the predicted system performance and sensitivity. Further, the team specified that the standards needed to be National Institute of Standards and Technology (NIST) traceable to certified reference materials. Inorganic Elemental Analysis (CST-8) designed and fabricated standards using packets of shredded paper impregnated with plutonium and americium at levels that were near the expected minimum detectable activities (MDAs). These standards, which are very similar in composition to the actual waste to be screened, have been used to test the performance of the WAND system for ^{241}Am- and ^{239}Pu-contaminated wastepaper. The plutonium and americium materials used for these

standards are NIST traceable: formal records were prepared establishing a quality assurance traceability for the standards. These CST-8 standards, together with some other standards (also NIST traceable) that were purchased commercially specifically for the WAND system and a number of previously acquired standards with a lesser degree of traceability, provide an extensive and very useful suite of standards for testing and confirming the WAND system's performance.

DOE Order 5820.2A[1] requires the Laboratory to segregate contaminated and uncontaminated waste. In a number of cases, the Laboratory has been unable to comply because it has not been able to prove that suspect waste is free of radioactive contamination. Of course, "free of radioactive contamination" must be defined, and we have had difficulty finding a set of coherent, reasonable criteria. As of July 1997, the DOE has not promulgated mass or volume limits for the free release of bulk materials such as waste paper and rags containing residual radioactive material. It is clear, however, that such limits should be expressed in terms of permitted mass concentration of contamination (i.e., contamination per unit mass). Knowing the measuring system MDA for various nuclides and the mass of the disposed waste would allow us to make a very conservative estimate of the upper limit of contamination going into a repository or dump.

Unfortunately, the only guidance available at this time is DOE Order 5400.5[2] (which deals primarily with surface contamination) and a 17 November 1995 memo from the director of the DOE Office of Environmental Policy and Assistance that attempts to clarify that guidance. As is reasonable, the stated criteria are expressed as surface contamination limits (units of activity per unit area). The clarifying memo states that mass or volume limits must be derived in a matter consistent with the ALARA process and with the surface limits stated in DOE Order 5400.5 and the clarifying memo; the limits must then be approved by DOE Headquarters or the cognizant DOE field office. As of August 1997, the Albuquerque Field Office has not given such approval. However, the LANL *Radiological Control Manual*[3] (see Table 2-2, Chapter 2) follows the DOE order and presents limits governing surface contamination, both removable and total, for all nuclides of interest. Those criteria are currently used at LANL for releasing people, equipment, or other items from controlled areas into uncontrolled Laboratory areas. In the case of people, they are obviously not only released into the uncontrolled areas of LANL, but are allowed to leave the Laboratory.

But, in practice, the limits are modified (or at least muddled) at LANL by the following statement in the LANL *Radiological Control Manual*: "It should be the goal of LANL that no items having levels of measurable contamination above natural background be knowingly released off site, for use by the public, even at levels below those of Table 2-2." This, of course, leaves the technical people wondering just what "measurable" means. At any rate, the dual criteria add to the complexity of segregating nonradioactive room trash from contaminated low-level waste. There are difficulties in applying the surface contamination limits stated in the *Radiological Control Manual* to what is fundamentally a contamination-per-unit mass problem. Actually interpreting the surface contamination criteria poses other

problems that are not yet resolved. However, Table 1 of DOE Order 5400.5, as interpreted by the administrators in authority, will govern the release of waste screened by the WAND system unless and until improved criteria are adopted. From the beginning, dating several years ago, the WAND team's goal has been to produce the most sensitive screening system possible (within what was thought to be a reasonable cost) in the hope that it would meet whatever release criteria were in effect at the time that the system was ready for use. The WAND team feels that, given any reasonable interpretation of the rules, the goal has been met. The following is a brief discussion defending this assertion.

WAND system MDAs vary with radionuclide (as well as with various setup parameters). With the WAND system set up to use 10-s counting intervals, the MDAs for ^{241}Am and ^{239}Pu are ~20 and ~300 disintegration's per second, respectively, for single, isolated, activity-bearing particles. These levels should be entirely adequate to justify burying the waste in ordinary landfills, as should the expected MDAs for many other radionuclides that might be encountered. (See Appendix A for details of a risk assessment study supporting this.) It should be noted that the MDA for ^{241}Am is much better than that for ^{239}Pu because the L x-rays of the former are emitted in 35% of the decays rather than in only 4.7% of them and because ^{241}Am emits a 60-keV gamma ray in 36% of all decays. These two nuclides represent almost the possible extremes, with most of the other nuclides of interest having MDAs between the ^{241}Am and the ^{239}Pu values, depending upon the photon emissions with which Mother Nature has endowed them.

If, on the other hand, the surface contamination criteria listed in Table 1 of the DOE Order 5400.5 are meant to define goals, the requirements need some interpretation. The smallest (i.e., most restrictive) number in the table is 20 dpm/100 cm^2 for removable activities of transuranics and seven other nuclides. A smear with 20 dpm of alpha activity is indeed readily detected with a properly shielded gas-flow proportional counter. There is no known system designed for bulk measurements, including the WAND system, that can detect 20 dpm on a single 100-cm^2 area.

However, because the x-rays and gamma rays that the WAND system detects have much better penetration than do alpha particles, many layers of paper can be examined simultaneously. For example, 75% of all L x-rays emitted from the bottom sheet of a stack of 27 sheets of standard 20-lb copy paper can penetrate the stack and be detected. Calculations based on measured detection efficiencies show that for a layer of paper 0.2 g/cm^2 thick that is *uniformly contaminated throughout its volume* (equivalent to 27 sheets of 20-lb paper) and of sufficient extent to fill the field of view of the six WAND detectors, the MDAs are 152 dpm/100 cm^2 for ^{241}Am and 2310 dpm/100 cm^2 for ^{239}Pu. If we assume that there are indeed 27 sheets of paper in the layer being examined and that they are uniformly contaminated, then the overall MDA corresponds to 2.8 dpm/100 cm^2 for ^{241}Am and 43 dpm/100 cm for ^{239}Pu on each of the 54 surfaces involved. The ^{241}Am value is, of course, far under the minimum value of 20 dpm/100 cm^2 given in Table 1, and the ^{239}Pu value is only a factor of two greater than the minimum value.

It is not clear to the WAND team why WAND performance should be compared to the minimum allowed value for removable activity, but because that usually seems to be the desire of those who inquire, we have presented the previous comparison. If comparisons to limits for surface contamination are made at all, we consider it more reasonable to compare WAND performance to the limits for total (removable plus fixed) contamination, all of which are greater by a factor of five or more than those for removable contamination. Both the DOE Order and its clarifying memo include some wording regarding the area over which measurements may be averaged. Depending on the interpretations thus far heard—and there is not yet any consensus—whether WAND meets the letter of the rules regarding area averaging depends on which of the various interpretations is agreed upon. It should be noted that smearing usually removes a rather small fraction of "removable" contamination and is, therefore, a very poor way (no way, in fact) to ascertain the amount of total contamination, which is, after all, the issue of ultimate interest in the disposal of waste. Clearly, the WAND system makes no distinction between removable and fixed contamination but instead measures total contamination within the limits of its capability.

Finally, we state again that we believe that the WAND system, given reasonable interpretation, meets any present guidance and (based upon formal risk assessment) can screen wastepaper and rags at sensitivity levels that fully justify their disposal in ordinary landfills.

II. GENERAL DESCRIPTION

The hardware portion of the WAND system basically consists of a lead-shielded chamber containing six large-area scintillation detectors. It has a conveyor system that moves a 12-in.-wide layer of paper (either shredded or in packets of up to 27 stacked sheets) through the chamber about 2 in. beneath the detectors and then dumps the screened material into a hopper. Packets of paper are manually placed on the belt or shredded paper is metered onto the belt by a hopper/auger system. The detectors are 5-in.-diam sodium iodide/cesium iodide phoswich scintillators of the type previously mentioned as being critical to the performance of the WAND system. Figure 1 is a general view of the existing WAND system, and Fig. 2 shows the inside of the detector chamber, with its six detectors.

The electronic portion of the WAND system comprises (1) all of the electronic modules—all purchased commercially except for one important custom-designed unit—needed to process the signals from the six detectors and (2) the small computer that processes the detector signals and controls the conveyer and auger systems. The computer now in use is a personal computer (PC) with a 486/66-MHz processor, adequate memory and storage capability, and a printer for producing reports. All of the electronic modules together occupy the equivalent of less than two, 12-slot NIM bins. Figure 3 is a photograph of all the system electronic modules, excluding only the computer.

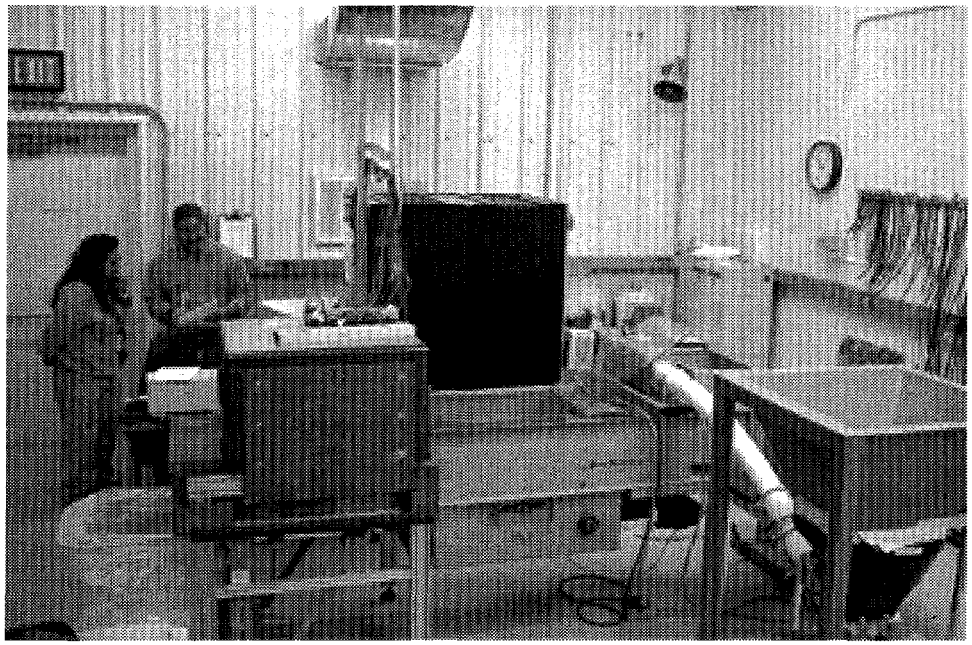

Fig. 1. General view of the WAND system (as it appeared in July of 1997). In the foreground are the lead-shielded detector chamber, the conveyor system, and the hopper through which shredded paper is metered onto the conveyor belt. In the background, with the operators, are the electronics racks and the computer which controls the system.

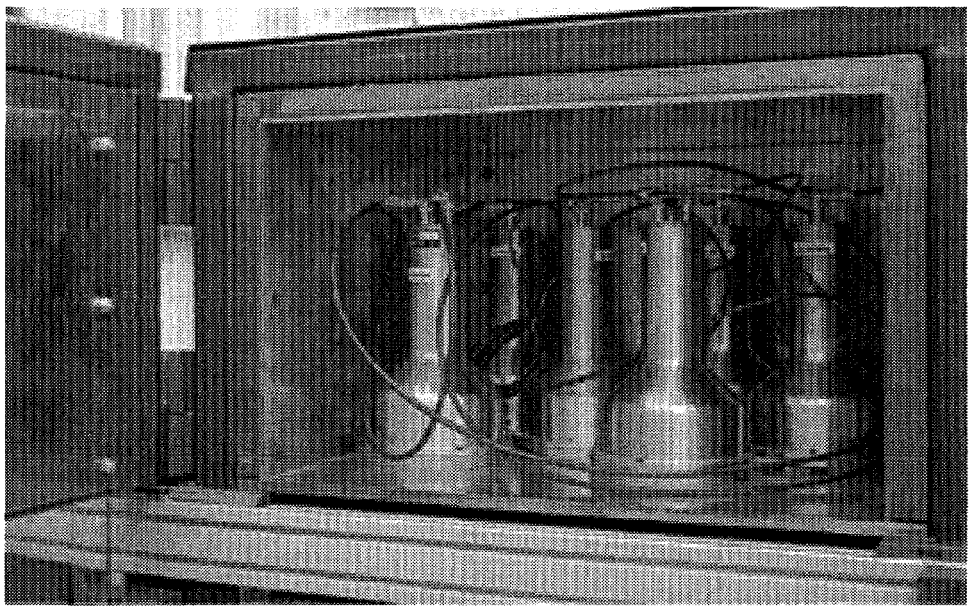

Fig. 2. The inside of the lead-shielded detector chamber, showing the copper lining and the upper parts of the six phoswich detectors.

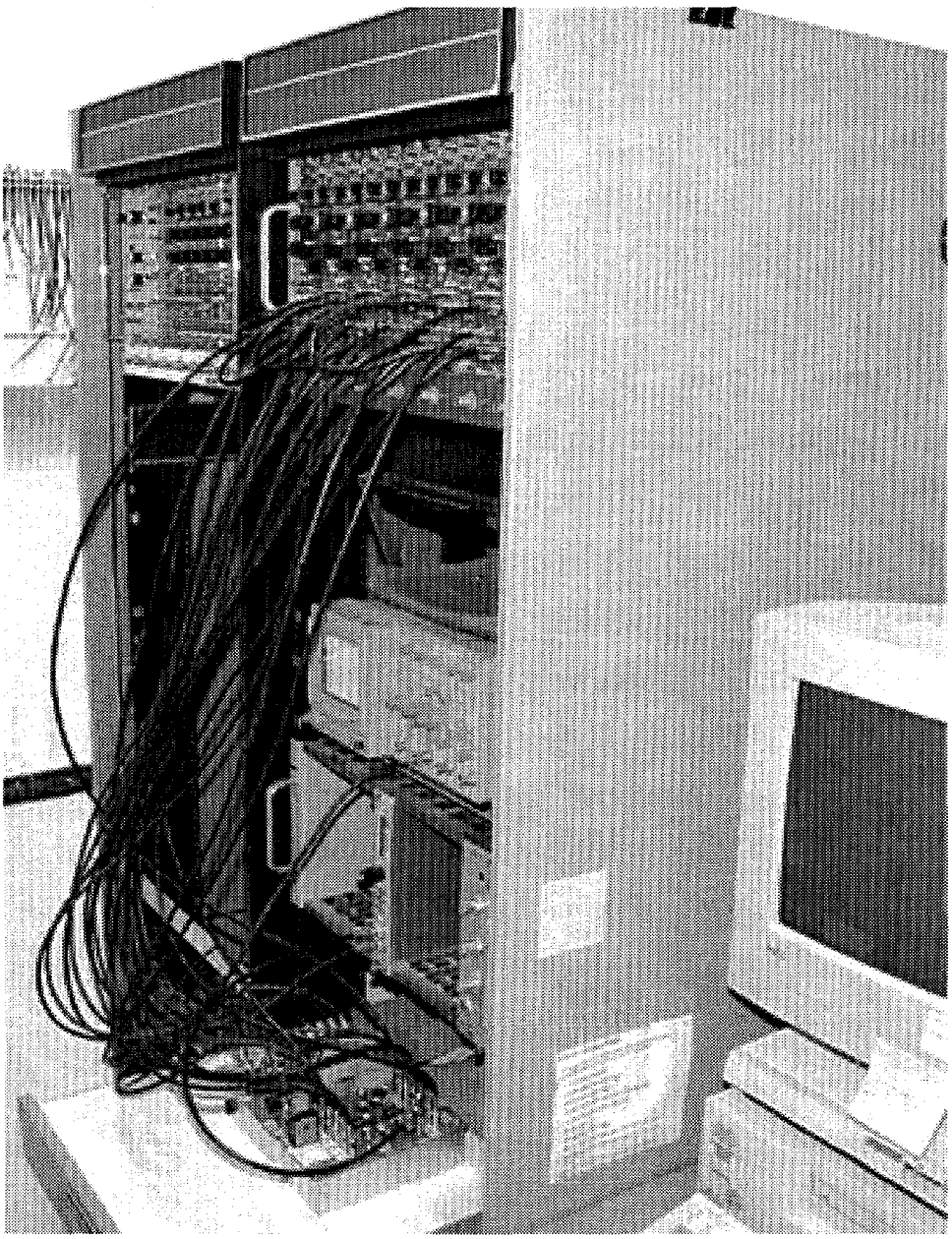

Fig. 3. The WAND system electronics. All the WAND system active electronic modules are in the near rack, including the custom electronic multiplexer and router at the bottom. The far rack contains only spare modules. The system computer is only partially seen at the lower right of the photograph.

The software portion of the system consists of the custom analysis algorithms coded in C++ language, along with all of the code by which the operator controls the system and produces reports.

III. DETAILED DESCRIPTIONS OF EQUIPMENT AND ANALYSIS METHODS

A. Descriptions of Hardware

1. Detectors and Shielding. The WAND system employs an array of six phoswich-type scintillation detectors. This detector type is so-named because each detector consists of a sandwich of two scintillation crystals that have different time constants for the emission of the scintillation light. We selected this type of detector because it offers high efficiency and lower background rates—by a factor of 4 to 5—than does any single-crystal alternative in the low-energy regions important to WAND. The phoswich detector also makes it possible to include photon energies ranging from 10 keV to about 1.8 MeV in the analysis because the sodium iodide and cesium iodide crystals have different energy calibrations.

The phoswiches used in the WAND system consist of a 3-mm-thick layer of thallium-activated sodium iodide that is optically coupled on one face to a 50.8-mm-thick layer of thallium-activated cesium iodide; each of these layers is 127.0 mm (5 in.) in diameter. The cesium iodide crystal is followed by a 9.5-mm-thick layer of optical-grade quartz that is coupled to a 5-in.-diam photomultiplier tube. To some extent the quartz shields the scintillator sandwich from gamma rays emitted by the radioactive contaminants in the photomultiplier; it also helps to smooth the response of the photomultiplier to light coming from different locations within the scintillators. The other face of the sodium iodide crystal is covered by an 0.001-in.-thick layer of aluminum. This "thin window" admits photons down to energies of ~10-keV with little loss, protects the hygroscopic sodium iodide crystal from moisture, and excludes light from the detector system. Figure 4 shows a mechanical schematic of the phoswich detectors, and Figure 5 is a photograph of one of the phoswich units.

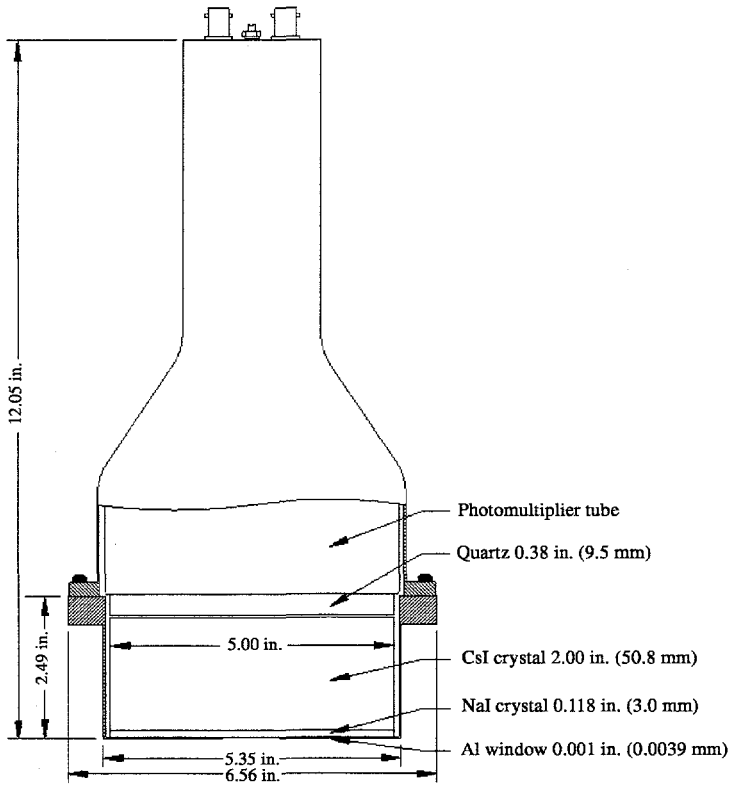

Fig. 4. A cross-sectional mechanical schematic of a phoswich detector, showing all the essential dimensions and the important structural parts.

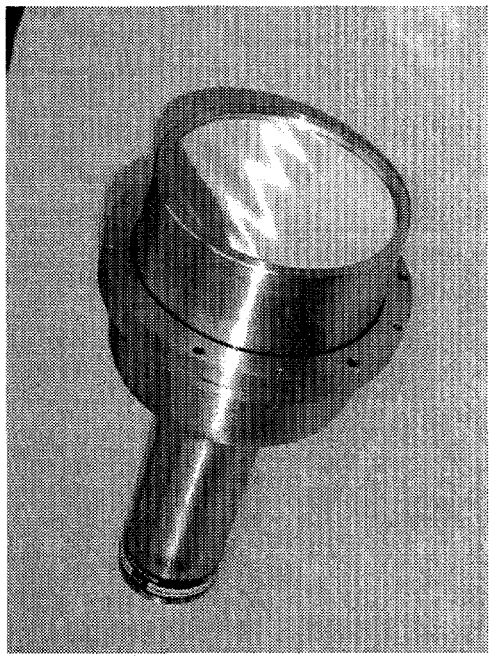

Fig. 5. A photograph of the exterior of one of the phoswich detectors, in which is seen the low-background copper shell and the 0.001 in.-thick aluminum window through which the detected photons pass.

The decay constant of the sodium iodide light is 0.23 μs, and the corresponding decay constant for the cesium iodide is 1.00 μs. The difference in the decay constants gives rise to different pulse shapes from both the preamplifier and the main spectroscopy amplifier. Those differences are exploited electronically so that events in which all, or nearly all, of the scintillation light is from the sodium iodide can be separated from those in which all, or at least a significant fraction, of the scintillation light is from the cesium iodide. Thus, higher-energy, Compton scattered events in the cesium iodide that could have created worthless background events in the important low-energy region of the sodium iodide spectrum may be eliminated. The sodium iodide background rates then decrease by factors of 4 to 5 compared to those created using an equivalent sodium iodide crystal with an inert light pipe the thickness of the cesium iodide crystal. Thin sodium iodide crystals backed by inert light pipes—usually called FIDLERS—are useful in many applications but do not offer the low background rates that the phoswiches can bring to the WAND paper-screening problem.

We should mention that thin sodium iodide crystals backed by inert light pipes were first used at least 20 years ago to reduce the background rates at low energies (plutonium L x-ray energies, in fact) relative to those produced by a thicker crystal. In the thin crystal, many of the higher-energy gamma rays pass through the crystal without interacting at all, thus reducing the lower-energy Compton continuum generated by thicker crystals. Crystals up to 50 mm thick have been used for waste screening by various investigators. They offer good high-energy efficiency, but they suffer higher background rates in the crucial low-energy regions. Figure 6 illustrates the ideas just discussed. It shows background spectra for three different 5-in.-diam sodium iodide detectors in identical shielding: 25 mm thick with a 25-mm-thick quartz light pipe; 1.6 mm thick with a 50-mm-thick quartz light pipe; and 3 mm thick with a 50-mm-thick cesium iodide crystal, as part of a phoswich detector. Of course, we used pulse-shape analysis (PSA) with the phoswich detector. As seen in Fig. 6, the 3-mm-thick sodium iodide detector that was used as part of a phoswich had background rates lower than those of the 1.6-mm-thick sodium iodide detector by a factor of 4 to 5 over the whole energy range. And, except in a short-energy region at ~100 keV, the thin 1.6-mm-thick crystal had significantly lower background rates than did the 25-mm-thick crystal. In that short region, the 1.6-mm-thick crystal rates were higher because some gamma rays passed right through it, Compton-scattered in the inert light pipe, and came back into—and were detected by—the thin crystal at lower energies. In the thicker crystal, the same gamma rays were detected as full-energy, or near-full-energy events, and were thus stored at higher-energy locations in the spectrum. Finally, if the FIDLER thin crystal had been 3-mm-thick, the superiority of the phoswich would have been even more apparent.

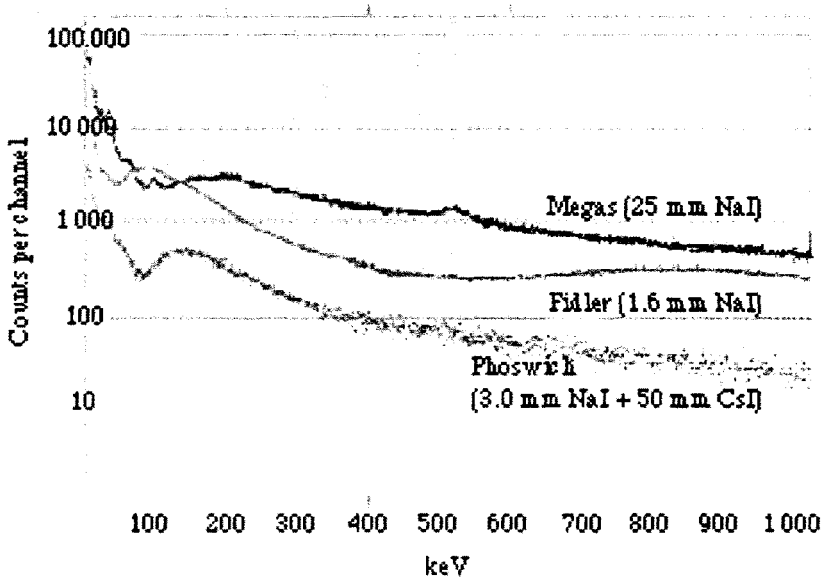

Fig. 6. Background spectra for three different 5-in.-diameter NaI detectors in identical shielding. It is evident that the 3-mm-thick NaI detector of the phoswich detector—which is used with pulse shape analysis—has significantly lower background rates.

Phoswiches offer a second distinct advantage in the effort to detect and identify the emitting nuclides of photons over a wide energy range. The phoswich detectors extend the possible useful energy range considerably because cesium iodide gives only about half as much light, but with a longer time constant, for the same energy deposition as does sodium iodide. This, combined with a further reduction in amplifier output pulse amplitude that results from the use of a short time constant in the spectroscopy amplifier, allows the cesium iodide spectrum to cover about 2.5 times the energy range of the sodium iodide spectrum.

As set up in the WAND system, the sodium iodide crystal spectrum extends up to ~750 keV, which allows the important low-energy region to be delineated with sufficient detail within the bounds of the 1024 channel spectra used in WAND. The cesium iodide spectrum, on the other hand, which extends up to ~1800 keV, includes almost all of the gamma rays from nuclides likely to be encountered at LANL. The 3-mm-thick sodium iodide crystal has very low efficiency for gamma rays above ~200 keV but is fully efficient for beta particles to the top of the ~750-keV range used in WAND. Indeed, it is fully efficient up to ~2 MeV for beta particles, though in WAND we do not use the beta range above 750 keV. The 50-mm-thick cesium iodide crystal has good efficiency for gamma rays up to the end of the ~1800-keV range used in WAND.

Figure 7 shows the preamplifier output of the phoswich when exposed to a source of ^{57}Co that has a principle gamma-ray energy of 122 keV. The differences in rise time and amplitude are clear. Figure 8 shows the bipolar output of the spectroscopy amplifier for a 1-μs time constant, when the output shown in Fig. 7 is applied to the amplifier. Again, the differences in output shape and amplitude are obvious. For the WAND system, it is the difference in the slope of the trailing edge of the bipolar outputs shown that we exploit for PSA. When

we subject the spectroscopy amplifier output to pulse height analysis, using PSA to separate it into the sodium iodide and cesium iodide spectra, we get the spectra shown in Fig. 9 for ^{57}Co. For reference, the unseparated spectrum is also shown. The 136.4, 122.0, and 14.41 keV ^{57}Co gamma-ray emissions visible in the spectrum have emission probabilities of 11.1%, 85.6%, and 9.8%, respectively. About three-quarters of the 122- and 136.4-keV ^{57}Co gamma rays interact in the sodium iodide crystal and one-quarter in the cesium iodide crystal, and the unresolved 122.0 plus 136.4 full-energy peaks are clearly visible in both spectra. The 14.41-keV gamma ray interacts only in the sodium iodide and so does not appear in the cesium iodide spectrum at all. It is evident that satisfyingly clean separation of the sodium-iodide-only events from all of the others has been achieved.

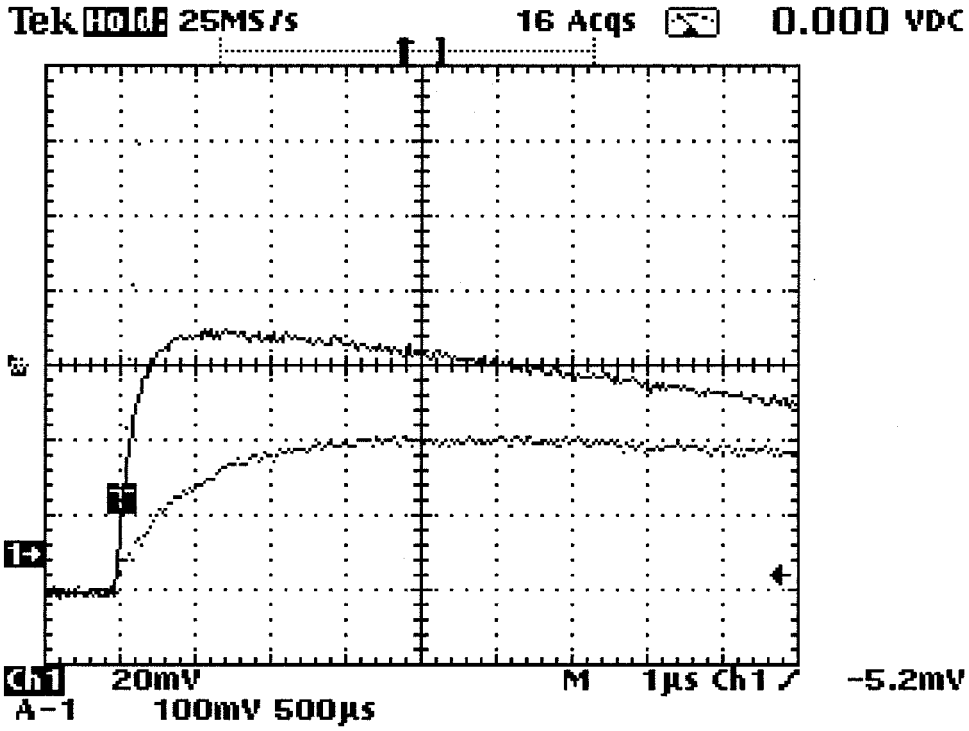

Fig. 7. The preamplifier output for 122-keV ^{57}Co events. The slower rise time and lower light output of the CsI portion of the phoswich are evident. Pulse shape analysis is based on the difference in rise time.

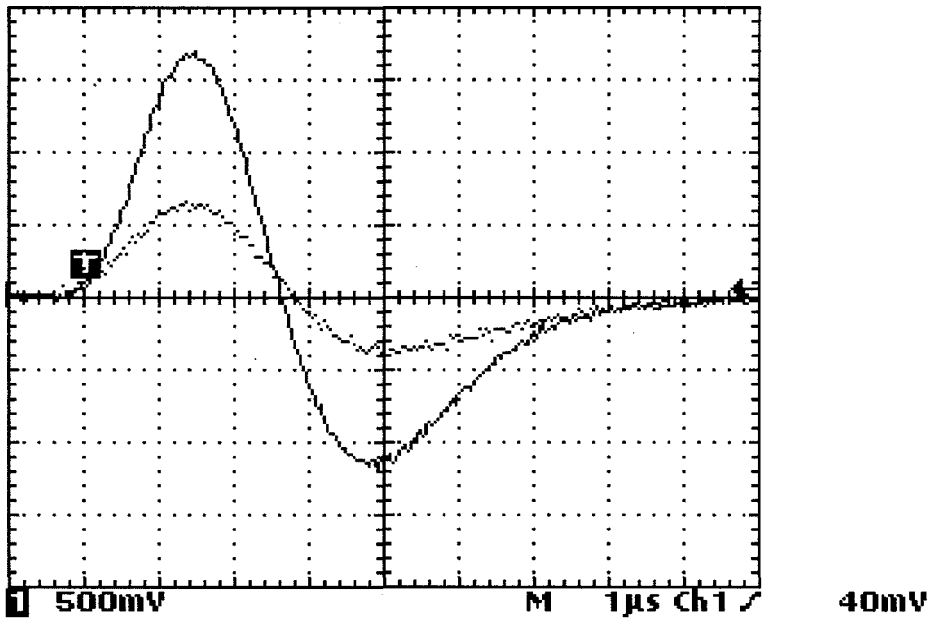

Fig. 8. The bipolar output of the spectroscopy amplifier—using 1 µs time constant—when the preamplifier output of Fig. 7 is applied to the input. Pulse shape analysis is actually accomplished by examination of the trailing edge of the positive lobe of the pulses.

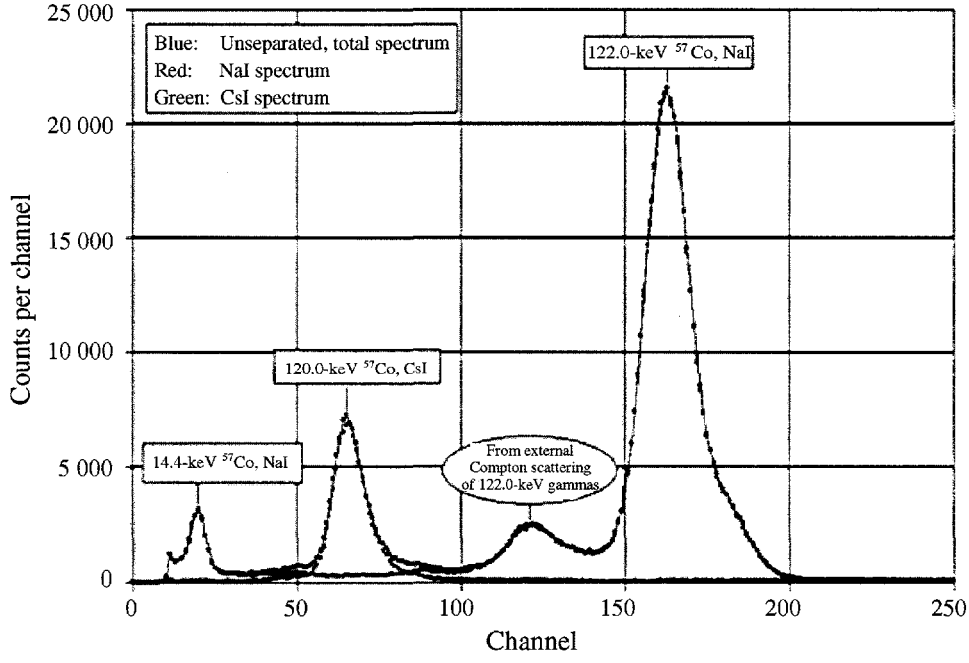

Fig. 9. The NaI and CsI spectra of ^{57}Co as separated from the total phoswich spectra by pulse shape analysis. The unseparated spectrum is also shown for reference. A clean separation of the NaI-only events from all others has been achieved.

We arranged the six phoswiches in the WAND system in the array shown in Fig. 10. We intended to achieve a reasonably uniform spatial response to activity in a 12-in.-wide (30 cm) layer of paper. The array comprises, in effect, two identical banks of three detectors. The two banks of detectors provide redundancy and lower MDAs when both banks are being used. The system could operate with a single bank, but the MDAs would be higher by a multiplicative factor of ~1.4. As we will discuss in detail further on in this report, this arrangement does indeed give reasonably near-equal responses—at least sufficiently so for screening waste—from identical point sources anywhere in the 12-in.-wide layer of paper. However, because the mechanical layout had to be finalized long before we had the opportunity to perform a detailed study of the spatial response to different geometrical detector arrangements, the layout is not optimal. Its near-optimal quality resulted from our somewhat lucky intuitive analysis of the physics involved. If further models of WAND are ever constructed, the layout of the detector array could probably be improved.

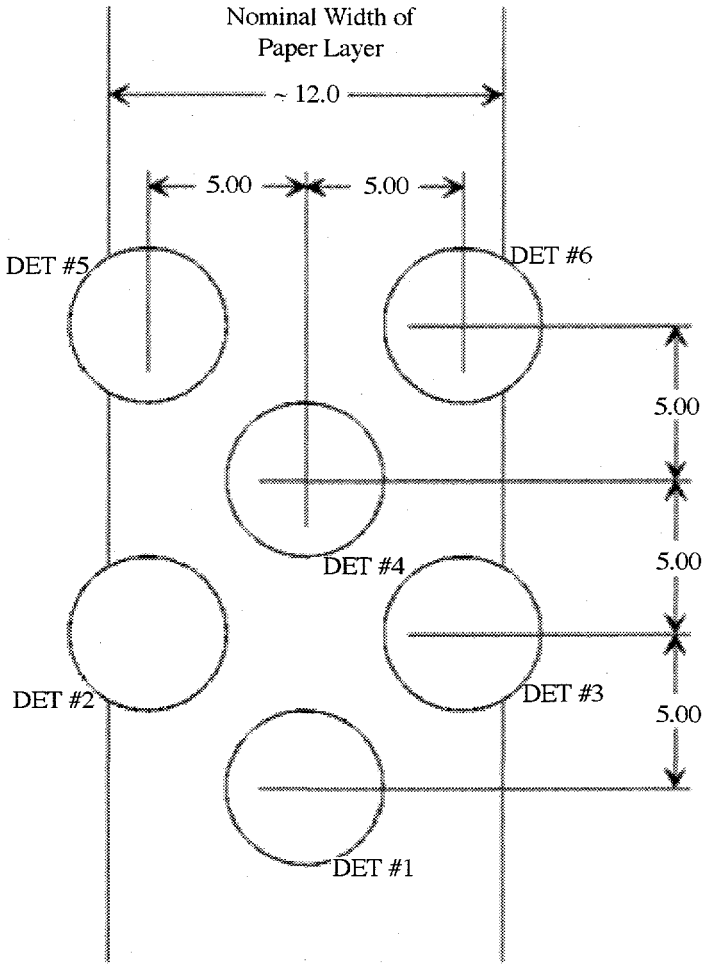

Fig. 10. The geometrical arrangement of the six 5-in.-diam phoswich detectors in the present WAND system.

To achieve low MDAs we must have low background rates in the detectors, which condition requires that the detectors be shielded from the ever-present background radiations as well as is reasonably possible. In the present configuration, the WAND detectors are surrounded by about 2 in. of lead, excepting the necessary penetrations for the belt that moves the paper beneath the detector array. In addition, there are layers of copper and cadmium of various thicknesses between the detectors and the lead. This shielding is probably adequate, though not ideal, for many applications; it could be improved in any future similar systems. Therefore, we will provide a short discussion of the principles involved.

The possibility of developing future similar systems brings up questions not only of how the shielding might be improved, but also of whether lead should be used. Current pressures from various sources to minimize or eliminate the use of lead as shielding—or to enclose it in aluminum, steel, or some other "safer" material—are motivated by safety considerations. It is our conviction that lead can be used with more than adequate safety and that there are strong technical reasons for using it, as we will now describe.

Remember first, that low-Z elements have much higher cross sections for Compton scattering (relative to photoelectric absorption) than do high-Z elements, especially at lower energies. Any low-Z material inside the main high-Z shield of the assay chamber—which we assume to be lead—will cause more Compton scattering of those background photons that find their way into the shielded assay chamber. Because all Compton scattering reduces the energy of the scattered photons, the presence of significant quantities of low-Z materials increases the low-energy part of the background spectrum relative to the high-energy part. When the inside of the assay chamber shielding is lead, there is a greatly increased probability that the photons that find their way into the assay chamber will be totally absorbed so that the low-energy regions of the spectra will have lower background rates. The problem is significant up to ~300 keV. As an additional reason for not encasing lead shielding in aluminum or steel, we cite the fact that unless these materials are very carefully purified or selected, they are not generally considered to be low-activity materials. It does not seem particularly wise to invest in a good primary shield and then place materials containing significant contaminant activities inside it.

Having said all the preceding about the deleterious effects of low-Z materials inside a lead-shielded assay chamber, we now assert that a thin liner of appropriate lower-Z materials is useful inside the WAND assay chamber. Any background photons with energies above 88.0 keV that are inside the chamber will excite lead K x-rays, which will create a large localized peak in the background spectrum. The energies of the lead K x-rays are from 72.8 to 87.3 keV. Of course, the finite resolution of the sodium iodide spreads the feature into a peak whose fringes are significant from perhaps 65 to 92 keV. If the K x-ray peak is too large, it will interfere with the very important region of interest (ROI) covering the 59.5-keV gamma-ray peak from ^{241}Am. In addition, all lead has traces of ^{210}Pb, which has a 46.5-keV gamma ray that will add to the low-energy background continuum. Finally, the L x-rays of lead fall in the 10- to 15-keV range, the lower part of the range in which any screening

system will be looking for the L x-rays from thorium, uranium, plutonium, americium, etc. Therefore, it is obvious that we should reduce the production of lead x-rays as much as possible, even if it causes the general low-energy background continuum to increase a little. A standard, much-used solution to the problem is to line the inside of the shield with a layer of cadmium ($Z = 48$) next to the lead, followed by a layer of copper ($Z = 29$). Frequently both layers are ~1/32 in. thick (~0.8mm), though the thicknesses may vary depending on how thoroughly the lead K x-rays are suppressed and how much extra general continuum is tolerable. The cadmium absorbs most, if not all, of the lead x-rays and emits 23- to 26-keV x-rays, which are subsequently absorbed by the copper; the copper x-rays have energies of only ~8.5 keV, which is below the energy range of interest for any NDA (nondestructive assay) system looking at the L x-rays from high-Z elements.

A slight caveat to the use of cadmium in the graded lining is that it has high cross sections for neutron absorption, followed by gamma-ray emission, which can measurably increase background count rates. For use in a plutonium facility, which has a neutron background that is far above the usual, the cadmium could be replaced by tin ($Z = 50$), a tactic that has sometimes been used to eliminate such neutron-capture gamma rays as a source of background. And although in sheet form tin costs much more than cadmium, it is far more acceptable from a safety standpoint than cadmium, which is poisonous.

In the WAND system, the low-energy range (up to, perhaps, 300 keV) is most important in obtaining highly sensitive screening of such nuclides as ^{239}Pu, ^{238}U, and ^{235}U. The screening sensitivity depends on achieving the maximum possible reduction in the background rates in that energy range. Figure 11 shows how strongly background rates depend on the completeness and thickness of the shielding. The figure shows three background spectra from the sodium iodide crystal of one of the phoswiches in the current WAND configuration, which was designed to confirm the cleanliness of clean wastepaper. In the highest-rate spectrum, the detector was shielded by a 1-in. thickness of lead in which there were some significant gaps. For the intermediate-rate spectrum, we added extra lead and blocked most of the gaps. The result was an ~1.5-in. average thickness of lead around the detector box. Note that this added lead thickness caused a major reduction in background rates. The ~75-keV lead K x-ray peak was prominent. In the lowest-rate spectrum, still more lead was added, bringing the shielding to a near-2-in. average thickness, and 1/32-in.-thick layers of cadmium and copper were added over most of the lead viewed by the phoswich detectors. This spectrum represents the "near best" that the present WAND system can achieve. Of necessity, there is a belt sliding on a steel plate to transport the paper beneath the bank of six detectors. Even though there are no line-of-sight paths from the detectors to the outer environment, significant numbers of low-energy photons reach the detectors through Compton scattering in the belt and the steel plate. Additionally, the box enclosing the detector photomultipliers is lined with 0.5-in.-thick copper plates, and the detectors are supported on an 0.5-in.-thick copper plate; thus, more copper than necessary is introduced over about half of the total solid angle. This situation (something that was locked into the existing prototype before we fully realized the consequences) means that the WAND

backgrounds are somewhat higher than the optimum. It also indicates that a system in which boxes of paper are measured in a completely enclosed shield container with optimized cadmium (or tin) and copper lining is likely to have a somewhat lower background than does the present WAND system.

We must mention one more consequence of the presence of low-Z material in the measurement chamber. The paper to be screened consists primarily of hydrogen, carbon, oxygen, and nitrogen and is, therefore, obviously low-Z. Variations in the amount of paper in the chamber will create small variations in the background spectrum. Background in the WAND system should obviously be measured with an "average" layer of paper in the chamber, but because the amount and composition of paper in the chamber will vary, the actual background rates will also vary. In the WAND system, in which there will usually be <500 g of paper at a time, the effect is small—probably ignorable in any practical way. In a system that examines 2-ft^3 (up to perhaps 15-kg) boxes of waste, the effect is not so small and will surely be one of the factors that limit accuracy and the accurate definition of MDAs. To illustrate the possible magnitude of the effect, Fig. 12 shows the sodium iodide background from a phoswich detector in a well-shielded chamber, both with and without the presence of a box of paper.

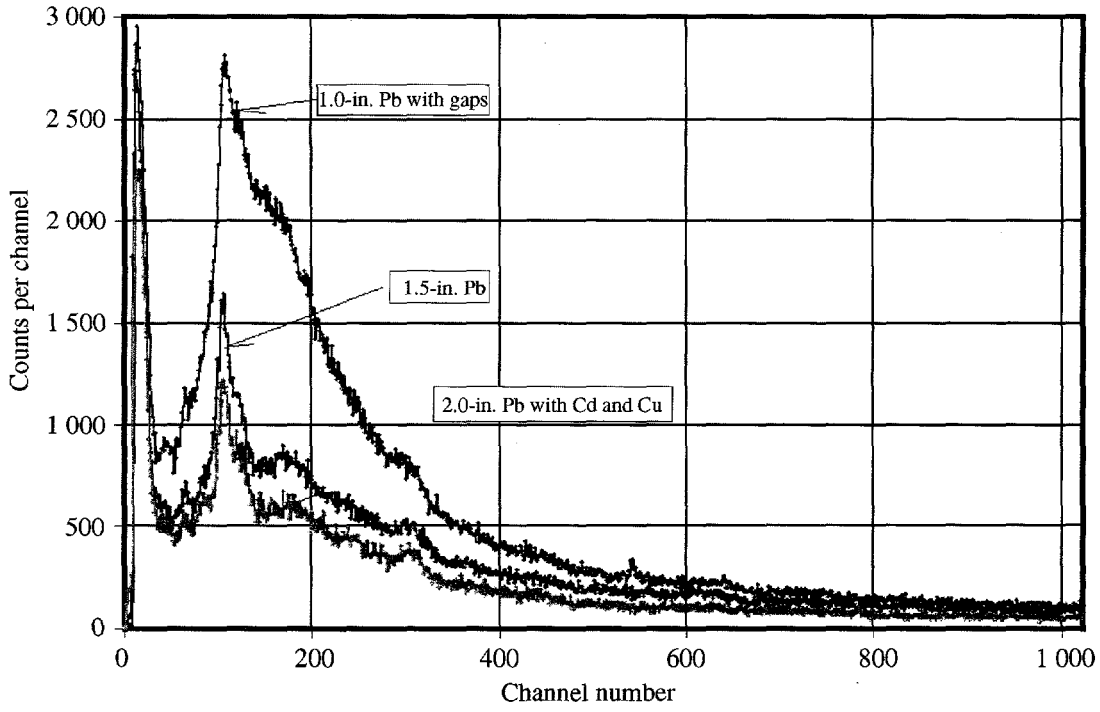

Fig. 11. The background spectrum of one of the WAND system detectors with varying thicknesses of shielding. It is evident that proper shielding is very important in achieving the low background rates which are essential to high-detection sensitivities.

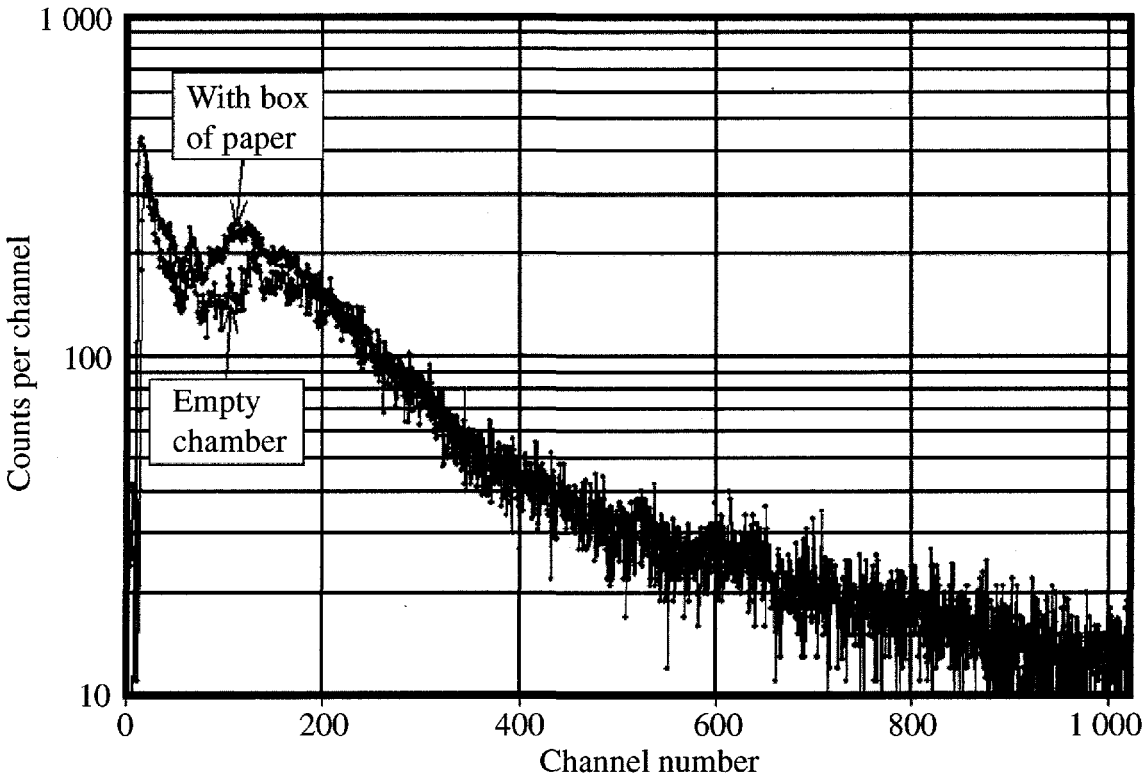

Fig. 12. Background spectra for a phoswich detector in a well shielded chamber, with and without the presence of a box of paper. This figure shows that the background spectrum is not an immutable constant, but depends to a small extent on the amount of low-Z scattering material in the measurement chamber, thus imposing a minor constraint on the possible accuracy of the measurement system.

2. Electronics. We made every possible attempt to use commercially available electronic modules for the WAND assay system. However, with six phoswich detectors, each consisting of a sodium iodide and a cesium iodide crystal, it was clear that we would need to combine signals and present them to the computer for analysis as a single spectrum in order to keep up with the data analysis in real-time. Each detector was equipped with a Canberra Model 2005 preamplifier and two NIM modules: an Ortec Model 572 amplifier and an Ortec Model 552 pulse-shape analyzer. These electronic modules provide the buffering, amplification, and PSA needed for the proper presentation of signals to the custom router module, which separates the sodium iodide and cesium iodide signals by their rise times and transfers this information into the computer-mounted multichannel analyzer, a Canberra Model S-100 system.

Our choice of the Canberra S-100 multichannel analyzer board mounted in the IBM-compatible computer was driven by the availability of support software. With the windows-compatible software, it was a straightforward task to provide the custom analysis of the data in real-time. However, the selection of the S-100 board dictated the requirements for the analog-to-digital (ADC) module, which had to be compatible with the S-100. We used a Canberra Model 8706 NIM module. In order to use a single ADC module for six dual-crystal

detectors while preserving the individual signals from each of the twelve detectors, we had to design a custom multiplexer module to handle the data. This custom unit, which is still essentially at the breadboard stage, is shown in Fig. 13. We anticipate that future developments will include commercializing this unit and packaging it in an NIM configuration, which can be done at relatively minimal expense.

The detector's preamplifier (Canberra Model 2005) derives its power from a cable attached to the amplifier module. Model 2005 is a charge-sensitive unit that collects the charge output (the anode signal) from the scintillation/photomultiplier detector's tube base and converts the signal to a positive one for presentation to the amplifier. The charge conversion gain of this preamplifier is nominally 4.5 mV/pC.

Fig. 13. The prototype custom multiplexer module designed for WAND. It reduces significantly the number of commercial modules required for the system.

The signal from the preamplifier is presented to the Ortec Model 572 spectroscopy amplifier, which accepts the signal and produces amplified outputs for input to the Ortec Model 552 pulse-shape analyzer and the custom multiplexer. The input impedance of the amplifier is ~500 ohms, which allows for the long cables that are necessary between the preamplifier and the amplifier in the present system. We must use the long cables because the preamplifiers are mounted at the detector shield cage, but the amplifiers are NIM units mounted in the racks with the computer, several meters from the detectors.

The Ortec Model 552 pulse-shape analyzer is a single-width NIM module. For this application it accepts as input the bipolar output of the spectroscopy amplifiers (Ortec Model 572) and provides two outputs necessary for the custom multiplexer unit: (1) an A signal, which occurs at the 90% point on the trailing edge of the positive lobe, and (2) a B signal, which occurs as the bipolar pulse passes through zero.

We use this module in the integral mode, for which we adjust the lower-level discriminator to the lowest point possible without triggering on noise in order to accept pulses with amplitudes as small possible, generally with energies <10 keV. Every time the discriminator is exceeded it provides an output signal through Channel A. The output, an NIM-standard, fast-negative output pulse, is generated by the constant-fraction method on the trailing edge of the input signal after the logic for acceptance has been completed. The fraction selected is at the 90% level of the trailing edge.

An output through Channel B is generated by the zero-crossover method. It provides both the fast-negative and the standard positive-going logic pulses, the latter of which are used by the multiplexer. In this way, the fall time of the input signal (which is proportional to the rise time of the signals from the detector preamplifiers) determines the time between the A and B outputs and serves to distinguish between signals from the sodium iodide and the cesium iodide detector segments by their rise times. The linear unipolar outputs from the ORTEC 572 amplifiers are delayed relative to the A and B outputs of the ORTEC 552 so that a decision regarding acceptance can be made on the basis of the A and B timing characteristics.

Whereas each of the six detectors requires a separate preamplifier, amplifier, and pulse-shape analyzer module, the A and B signals from the ORTEC 552 now combine with the unipolar pulse from the ORTEC 572 in a single "wand router" custom module for use by the ADC and the S-100 multichannel analyzer. The wand router accepts the three signal inputs from each detector channel for a total of 18 inputs. It provides a linear output to the ADC, routing (address-line) signals to the S-100, and several diagnostic signal outputs.

The wand router operates as follows. The A channel inputs go into a front-end processor that determines which of the inputs has been struck and that guarantees only one of them will be struck at a time. This potential limitation in count rate is not significant in the present system because very low count rates are involved. The dead time incurred by allowing only single detector signals for processing is not a major limitation at total count rates below

~20 kHz. This front-end processor provides the address of the channel that was struck and, then, gates the analog multiplexer for the unipolar inputs and the multiplexer for the B signal inputs. In this way, the system guarantees that for a given A signal, the unipolar and the B signals will be from the same detector. These same address lines provide three address signal inputs for the S-100, thereby guaranteeing that a given signal will be stored in one of the two spectral segments reserved for the detector. Having now determined which of the eight spectral-segment pairs will store the signal value it must be determined whether the signal should be put into the higher sodium iodide spectrum region or the lower cesium iodide region. This determination is based on the intervals between the A and the B output signals from the ORTEC 552. Those intervals are rather cleanly separated into two groups, one that is associated with sodium iodide events and one with cesium iodide events. The coincidence of the former group with a univibrator generates the required fourth routing bit. In this way, the 16-K S-100 spectrum is divided into sixteen 1-K segments. All the sodium iodide signals end up at the top end of the 16-K spectrum in the ninth through fourteenth 1-K segments. The cesium iodide signals end up in the first through sixth 1-K segments of the spectrum.

The unipolar analog signal exits the analog multiplexer and is routed to a peak detector and stretcher for presentation to the ADC. When the peak detector determines the peak of the signal, it sends a request to the ADC to convert the signal. The ADC provides the digital address lines to the S-100, which determines which of the 1024 channels in the prescribed segments will be incremented.

The width and delay of the pulse that selects the events to be stored in the sodium iodide end of the spectrum are adjusted by potentiometers on the multiplexer circuitry. Those adjustments are critical to ensuring that the sodium iodide pulses are cleanly separated from the cesium iodide signals.

3. Mechanical Subsystems. There are actually three main mechanical subsystems in the WAND instrument: the paper shredder, the auger feeder, and the conveyor system. The shredder is a stand-alone unit whose purpose is solely to generate shredded, low-density paper waste that we can place in a uniform layer on the conveyer for analysis. Any heavy-duty unit can be used. We used an Ameri-Shred Model EBA 400 unit (with a 4-hp motor), which yields a particle size of 3/32 in. × 1/2 in. and has a capacity of 10–20 sheets/pass (minimum 40 cubic feet per day of crumpled paper) and a cutting speed of 81 feet per minute.

The auger system automatically spreads a uniform layer of shredded paper across the conveyer. However, to function properly, the system requires considerable mechanical custom-tuning, and in many cases we found it simpler to spread the paper by hand on the conveyer.

The conveyer is the heart of the mechanical assembly because it provides the means of moving the paper under the detector bank at a uniform and adjustable rate. It is also computer-controlled for automatic operation. We purchased an industrial conveyer from

Ameri-Shred Industrial Corporation: Model C-50-10 came equipped with a 22-in.-wide by 24-ft-long neoprene nonstick belt. It uses a 1/2-hp dc motor with an average speed of 1 foot per minute. We built an interface between the controller and the computer to enable the computer to vary the speed between ~1 cm/min and ~1 cm/s and also to reverse the belt upon demand. These capabilities enable the computer not only to determine whether the waste under study has any measurable contamination, but also, in the case where a count equals or exceeds the critical level (LC) that indicates excess activity, to reverse direction and take the measurement again.

False alarm events are thereby identified in almost every case so that we no longer need to dispose of clean material in the hot dump. The reason that there is an expected and acceptable rate of false alarms to be dealt with will be explained later in this report.

The conveyor includes one bag, mounted on a mechanical holder, into which it automatically dumps the wastes after the assay so that the operator no longer needs to handle the waste after the assay is complete.

B. Descriptions of Methods and Analysis Algorithms

1. Definitions of MDA and Related Concepts. Reference has previously been made to the concept of MDA. However, aside from the qualitative implication that it is a measure of the minimum activity that can reliably be detected, it has not been as carefully defined as it deserves. This is particularly important because those who do low-level counting of radioactive materials have used many different definitions, whose values have varied by at least factors of 2. After we establish our definitions, we can better assess the validity of the claims made regarding the WAND system and more accurately compare its performance with other systems.

Whenever we count discrete events as a measure of radioactivity, we must establish a rate (or a number) that, when equaled or exceeded, is declared to indicate excess activity beyond that which caused the observed background. This declared quantity is called the critical level (LC). It is usually expressed as a net rate (a gross rate minus the background rate), though this is not necessary and sometimes not even desirable. In the WAND system, in fact, we *use the total (rather than the net) number of counts* observed in the short-counting intervals employed; the terminology used in the rest of the discussion will reflect this usage. The value of the LC will therefore be a positive integer because we do not ever subtract a background from the integer number of counts that we observe in the counting intervals. This approach is advantageous because we use the Poisson statistical distribution to calculate all probabilities used for analysis in the WAND system. The Poisson distribution is most appropriate for the rather small integer count numbers (generally <10) that we observe in the short-counting intervals that we employ. The basic properties of the Poisson distribution are given in Appendix B.

The LC is usually set low enough that the fluctuations in the pure background will occasionally cause observed counts equal to or greater than the LC, thereby instigating a spurious declaration of detection, or a "false alarm." On the other hand, contaminant activity levels that cause average counts equal to or greater than the LC can, again because of statistical fluctuations, sometimes yield observed counts less than the LC, and therefore fail to be detected. From the average background count, which is usually determined as the average of many normal counting intervals, we can calculate the probability that an observed count will occur in a single, relatively short measurement of background. We therefore calculate the LC based on the fraction of false detections of activity that we are willing to accept. Further, based on the average background count and the agreed-upon LC, we can calculate the probability that any higher average count will result in a measured quantity less than the LC. Therefore, we must decide what fraction of detection failures to accept and then calculate the corresponding average count. This average count, which corresponds to the agreed-upon acceptable failure-to-detect probability, is usually called the detection limit (LD).

The MDA is proportional to the difference between the LD and the average background count. Thus the MDA is the contaminant activity that raises the average count (including background) to LD. The MDA is almost always much greater than the difference between the LD and the average background count because all of the radioactive decays in a contaminant source are rarely detectable. In the WAND system, in fact, the six phoswich detectors detect only fractions on the order of 10% to 15% of the photons from a particle directly under the detector. Note that the MDA is usually different for different contaminant nuclides because (1) the particular gamma rays or x-rays that the assay is based on have different probabilities for emission, and (2) detector efficiency and sample self-attenuation are variable functions of energy. Thus, a separate MDA is usually necessary for each contaminant nuclide of interest.

The above discussion shows that for every stated MDA there is an accepted nominal probability for false detection and an accepted probability for failure to detect. In practice, for low-level measurements both of these probabilities are often set at 5%; however, that is unnecessary and often undesirable. It should be mentioned that a frequently used definition of "sensitivity" (a term with roughly the same meaning as MDA) is the average net count equal to three standard deviations of the average background count. It is almost always used without mention of either the probability for false detection or for failure to detect, but yields values near those for LD, using the commonly assumed value of 5% for both the probability for failure to detect and for false detection. Both the LC and LD can be set so high that the probabilities for both false detection and failure to detect are essentially zero, but this is rarely, if ever, done. For both probabilities, finite values are almost always assigned because they are considered to be the most efficient and useful.

In the WAND system a great many short (~10-s) counts are made. Using a nominal accepted false-alarm probability of 5% would result in an unacceptably high number of false alarms. The false-alarm probability per spectral region of interest for each detector has been set at a nominal value of 0.001 in order to reduce the false-alarm rate to a reasonable value. On the other hand, we can reasonably use 0.05 for the overall failure-to-detect probability for a point source passing through the six-detector system. The complications involved in computing the overall failure-to-detect probability in a multidetector system will be dealt with further on in this report. Figures 14-17 aid in conveying the magnitudes and behaviors of the LC and LD. In Fig. 14, for a nominal false-detection probability of 0.001 and a failure-to-detect probability of 0.05, the LC and the LD are plotted as functions of the average background value N_{av}, for $0.1 <= N_{av} <= 25$. Note first that the LC has only integer values, a reflection of the fact that the number of discrete events counted in a fixed interval is, of necessity, an integer. The *average* background count can be nonintegral. The LD is an average number and can, therefore, also be nonintegral.

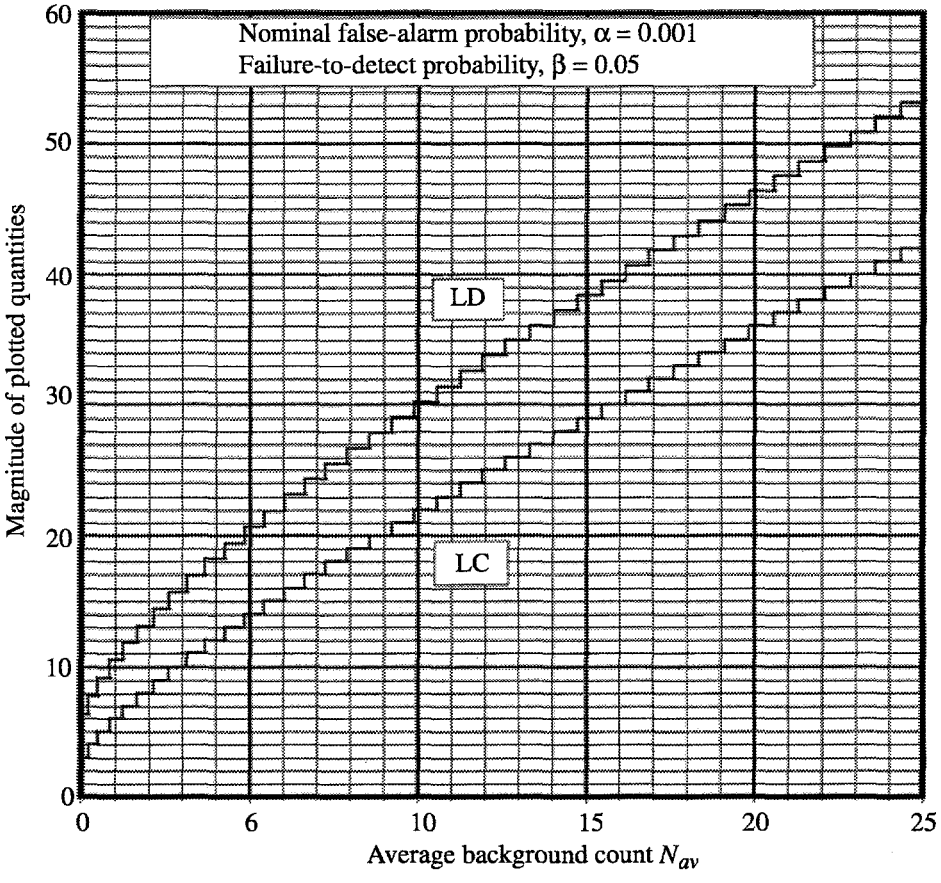

Fig. 14. The Critical Level (LC)and the Detection Limit (LD) as functions of average background count for a nominal false-alarm probability of 0.1% and a failure-to-detect probability of 5%.

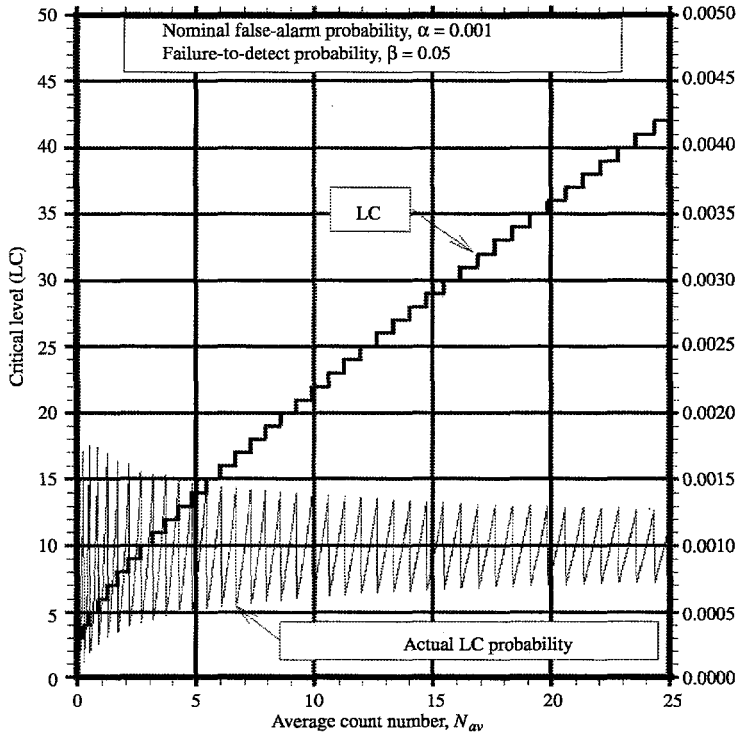

Fig. 15. The Critical Level (LC) and the actual false-alarm probability as functions of average count for a nominal false-alarm probability of 0.1% and a failure-to-detect probability of 5%.

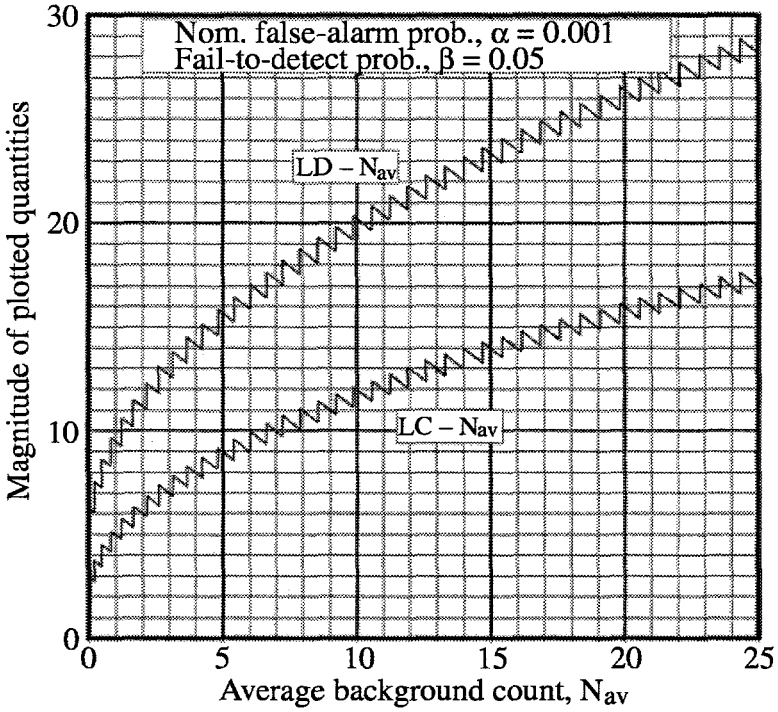

Fig. 16. Critical Level (LC) less average background count and Detection Level (LD) less average background count as functions of average background count.

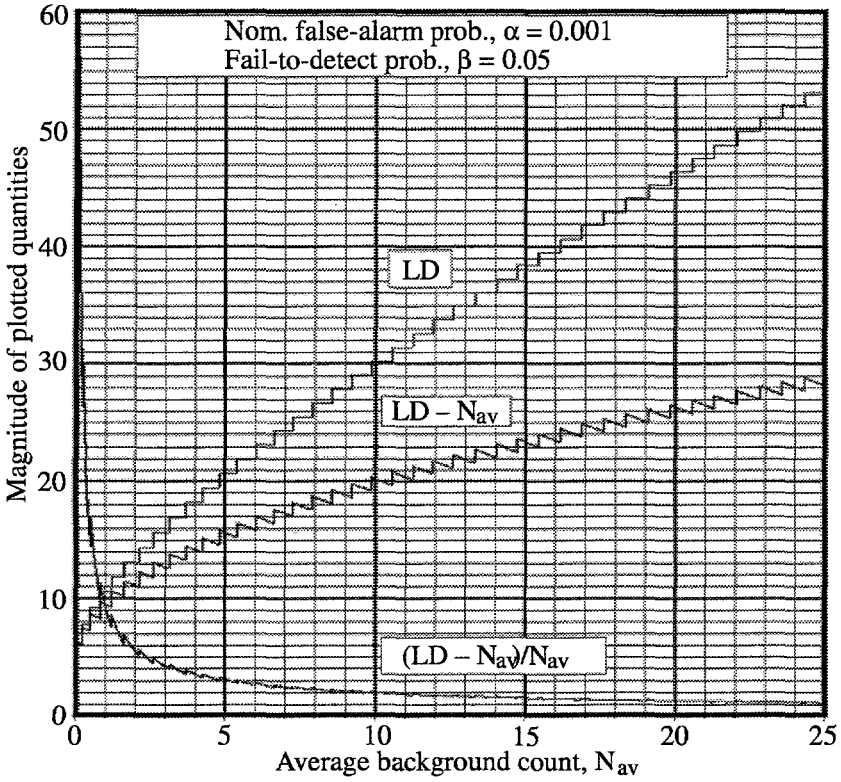

Fig. 17. Relationships involving the Detection Limit (LD) and the Average Background Count (N_{av}). We present LD, (LD – N_{av}), and [(LD – N_{av})/N_{av}] as functions of N_{av}. Note that the latter quantity systematically decreases and asymptotically approaches a value near 1.0.

We have emphasized that one selects a nominal acceptable false-alarm probability. The actual probability for false detection will almost never be exactly the nominal value, but will be either higher or lower—for small values of average background count, the fractional difference can be surprisingly large. In Fig. 14, the LC values are those whose actual false-detection probabilities are closest to the nominal value of 0.001. Figure 15 shows both the LC and the actual false-alarm probabilities that correspond to the values of the LC. Note that for the lowest average number corresponding to a given integer value of the LC, the probability is lower than the nominal value. As the average number increases to the highest value that corresponds to the selected LC, the false-alarm probability increases through and above the nominal value. As an example, LC = 8 corresponds to N_{av} values in the range of 1.67 to 2.13, with the false-alarm probability ranging from 0.00035 at the low end of the range to 0.00162 at the high end. This is consistent with the properties of the Poisson distribution, though the magnitude of the variation is somewhat surprising. It is clear that in the WAND system (and in any similar system recording low-integral counts) the actual false-alarm fraction will depend on where N_{av} is in the range that corresponds to the LC. As will be explained later, this is not a significant problem with WAND. Efficient procedures for dealing with false alarms are in place.

For the WAND system, both the LC and the LD include N_{av}. It is of interest to plot the excess counts above background that are needed to give both the LC and the LD, particularly because the difference between the LD and N_{av} is proportional to the MDA. Figure 16 gives these values, again plotted against the average background value N_{av}. We expect the MDA to be a function of N_{av} and the nominal false-alarm probability, but it is perhaps surprising that it is the sawtooth function shown in the figure. The observed behavior is, of course, a consequence of the small integer values of the observed counts. In situations where the observed counts are large ($N_{av} > 10$), the normal statistical distribution is easy and convenient to use in formulating analytic functions for the LC and the LD. Currie[4] and Lochamy[5] present such expressions, which give the impression of being smooth functions; the discontinuities are indeed relatively small, but they will still exist. When we use the Poisson distribution, we cannot formulate analytic functions for the LC and the LD. The calculations must be done numerically, but they are straightforward and quickly done with PC-type computers. There is no longer any reason to avoid the use of the Poisson distribution because of calculational difficulties.

Finally, in Fig. 17, we give the LD, (LD – N_{av}), and (LD – N_{av})/N_{av}. Note that the difference between LD and N_{av}, expressed as a multiple of N_{av}—[(LD – N_{av})/N_{av}]—systematically decreases and asymptotically approaches a value near 1.0.

2. Background Spectra and Background Rates. The WAND system's primary purpose is to confirm that clean wastepaper is truly clean with high sensitivity. Of the parameters governing the MDAs, the most important ones that can be obtained with the WAND system are the background rates in the spectral energy regions containing gamma or x-rays of particular interest. Because of this and because background is essentially all that the system will see when it is in use, the background spectra are of great interest. There are, of course, two background spectra for each detector, the most important being the one that consists almost wholly of interactions only in the sodium iodide detector. The other consists of interactions that are wholly in the cesium iodide detector or that generate significant scintillation light from both crystals.

In the shielded detector box, all the detectors have very similar background spectra. Both the sodium iodide and the cesium iodide spectra are digitized into 1024 channels, but they have different energy calibrations. As previously mentioned, the sodium iodide spectra use an energy calibration that is nearly E(keV) = 0.75 * Channel, which implies that they contain energies up to ~768 keV. For reasons previously discussed, the energy calibration of the cesium iodide spectra is different and reaches up to nearly 2000 keV. Because the light output of the cesium iodide per unit of energy relative to that of the sodium iodide differs slightly from detector to detector, there are significant variations in the exact energy calibrations among them.

Figure 18 shows, with a linear vertical scale, both the sodium iodide and the cesium iodide spectra from detector number 6 in a background count of ~220,000 live seconds. Several

things are immediately obvious. The first is that the overall rate in the former spectrum is much lower than in the latter. This is because the sodium iodide crystal is only 3.0 mm thick, while the cesium iodide crystal is 50 mm thick and because the PSA operates in such a way as to eliminate from the sodium iodide spectrum those events in which there was interaction in both crystals. The overall rate in the sodium iodide spectrum is 4.1 s^{-1}, while it is 28.1 s^{-1} in the cesium iodide spectrum. In both spectra there is a broad peak near Channel 100, which is caused by the Compton scattering of higher-energy gamma rays. We will not enter into a discussion of Compton scattering, but will only say that the spectral feature is both expected and inescapable. In the cesium iodide spectrum there are three distinct spectral peaks centered at 511, 662, and 1462 keV. The 511-keV peak is from the annihilation of positrons created in the pair production interaction of gamma rays of energies >1022 keV. The 662-keV peak is from ^{137}Cs, a contaminant in the cesium iodide crystal—it being essentially impossible in these times to get cesium iodide without a trace of ^{137}Cs. The 1462-keV peak is from ^{40}K, an almost inescapable contaminant in the glass of the photomultiplier tubes and in other materials present. The sodium iodide spectrum has a peak at ~75 keV that arises from K x-rays fluoresced from the lead shielding. By using 0.032-in.-thick layers of cadmium and copper between the lead and the detectors, we have reduced, but not completely eliminated this peak. Finally, in the sodium iodide spectrum there is a distinct upturn in the spectrum at energies < ~25 keV that arises from the scattering (and probably multiple scattering) of lower-energy photons and that is very hard to reduce. This can best be seen in Fig. 19, which shows just the first 200 channels of the spectrum of Fig. 18.

Presently, the WAND system software analyzes four distinct regions of interest to determine if radioactivity is present in the wastes traveling beneath the detectors. Three regions of interest are set in the sodium iodide spectrum, and one is set in the cesium iodide spectrum. In the former spectrum, ROI 1 is placed to detect low-energy x-rays (12–21 keV), ROI 2 is placed for the detection of ^{241}Am gamma rays (59.53 keV), and ROI 3 is set to detect penetrating beta particles (> 75 keV). This ROI is only 105 keV long, and many beta emitters will produce events at higher energies than those included in this ROI, but this choice gives an overall near-optimum sensitivity for all detectable beta emitters. ROI 4 is set in the cesium iodide portion of the spectrum around the 661.6 keV gamma ray from ^{137}Cs, (the most common fission product found in LANL wastes). More specific regions of interest could and should be placed to detect particular emissions, as well as one or two general ones. The locations of the three sodium iodide regions of interest are indicated in Fig. 19. The location of the 661.6-keV ROI is shown in Fig. 18.

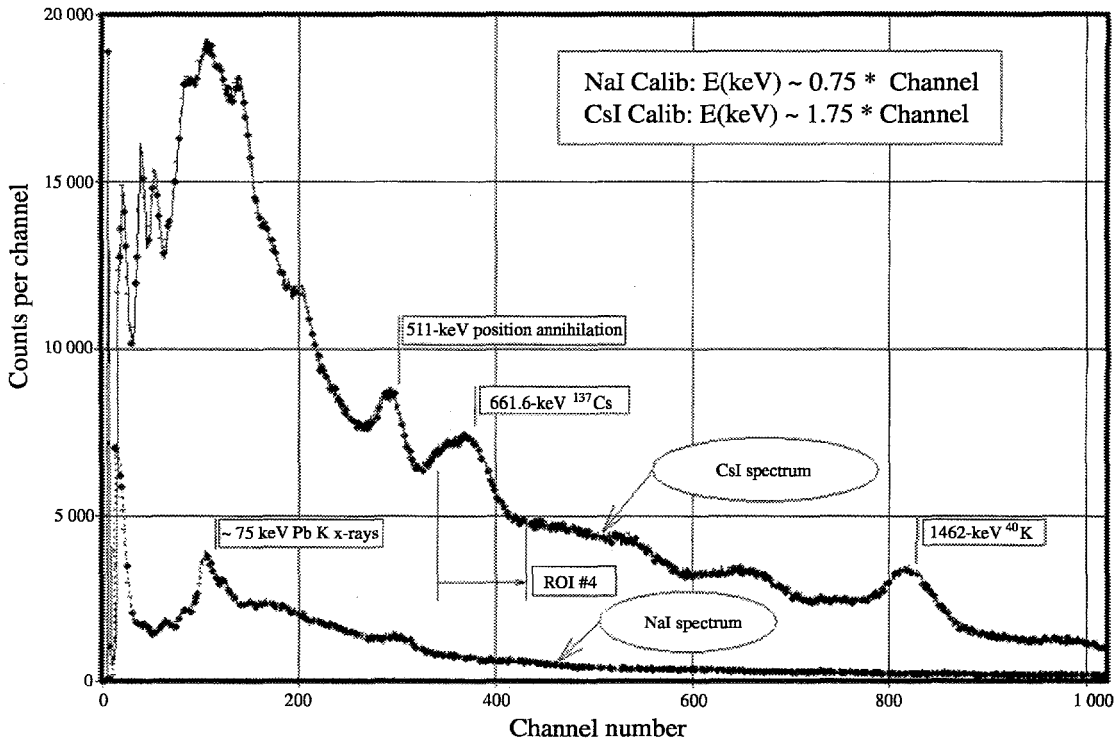

Fig. 18. The NaI and CsI background from the WAND system's phoswich No. 6. The position of region of interest No. 4, used to monitor the presence of ^{137}Cs, is shown in the CsI spectrum.

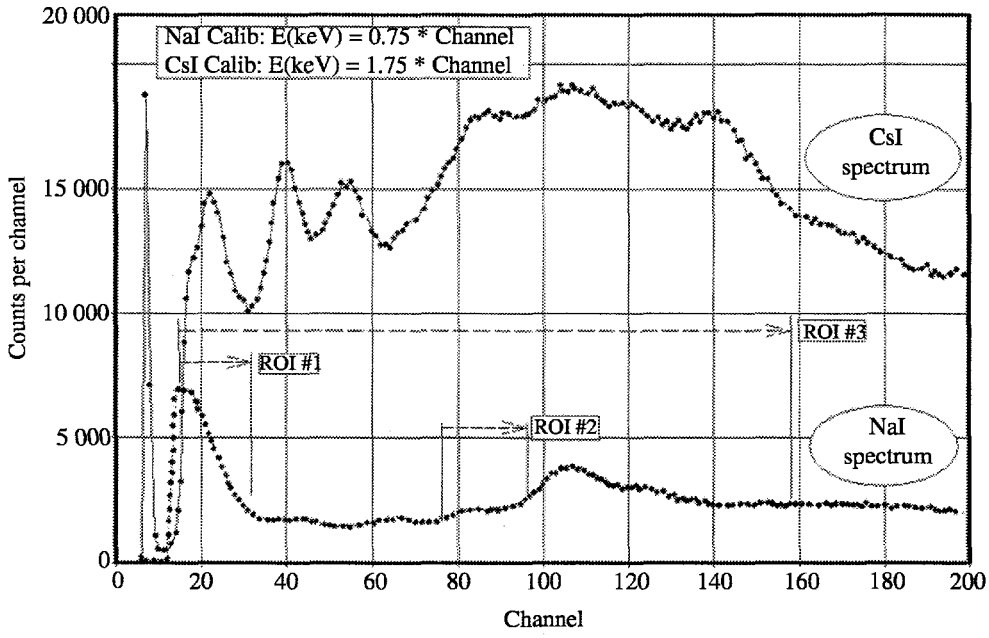

Fig. 19. The first 200 channels of the spectra of Fig. 18, shown in order to more plainly delineate the low-energy structure of the spectra. The positions of the first three regions of interest used in the current analysis are shown.

Average background rates (s^{-1}) for each of the four regions of interest in the six phoswich detectors are presented in Table I. The average background rates were measured from a series of 65 different 40,000-second counts made over a period of 5 months. It is worth noting that the higher background rates in PW1 occur because it is physically located closest to the input opening of the shielded detector box. Background rates in the WAND facility vary significantly more than simple Poisson statistics would predict. We are confident that this is due to fluctuations of a key background radiation source, the daughters of ^{222}Rn. Therefore, we evaluate standard deviations of background using an equation for the sample standard deviation of a Gaussian distribution.

Table I. Average Background Radiation Rates for WAND System Phoswich Detectors

Detector	ROI 1 Rates (s^{-1})	ROI 2 Rates (s^{-1})	ROI 3 Rates (s^{-1})	ROI 4 Rates (s^{-1})
PW1	0.4048	0.2265	2.6841	2.3304
PW2	0.3868	0.1807	2.0692	1.7779
PW3	0.3770	0.1838	2.0583	1.9271
PW4	0.3463	0.1821	2.0220	2.0462
PW5	0.3821	0.1855	2.1273	2.0118
PW6	0.3934	0.1851	2.1298	2.0369
Average	**0.3817**	**0.1907**	**2.1818**	**2.0217**

3. Computation of MDAs. In this section we describe how to calculate the MDA for a *single-point source* of activity passing through the system. We will then briefly indicate the modifications to the procedure that are required to calculate the MDA for a uniform surface activity. The latter calculation is not as important as the former because uniformly contaminated waste probably does not exist in the real world. The problem is of interest, however, because of the previously mentioned limits for surface activity that are currently being forced to fit the bulk-wastepaper problem.

For a multidetector system, we define MDA as the point activity that has the specified probability β of not being detected as it passes through the entire system. Remember that the MDA is a function of the following: the background rate in the ROI being considered, the nominal false-alarm probability, the accepted failure-to-detect probability, detection efficiencies, belt speed (which governs the length of time a source is viewed by the detectors), the emission probability for the gamma ray or x-ray being considered (the fraction of decays emitting the gamma ray or x-ray, which in most cases is less than one), the distance of the point source above the belt (which varies because of the finite thickness of the paper layer), the possible attenuation within the layer of paper, and the position of the activity on the belt relative to the detectors at the beginning of the counting intervals. There is more than one way to analyze the multidetector data. Two analysis methods are described here along with the advantages and disadvantages of each.

Clearly, we cannot calculate MDAs for even a fraction of the possible combinations of variable parameters, but we will calculate them for average and worst cases using what we expect to be the normal operating parameters. By doing so, we can obtain a feeling for the range of MDA values to expect. The variation with position on the belt is of particular interest to us, and we have written codes to study that variation, assuming selected sets of all the other parameters.

Currently, we analyze the multidetector data by what we term the independent detector method. In this method, we independently treat the counts from every detector during all of the count intervals when the source is in view. This method appears to be the obvious first choice, but it may not be the most advantageous. In a second method, which we term the prescribed sequence method, we take advantage of the fact that radioactive particles travel along the belt at a known speed. Intuitively, it seems clear that if the data are added together for prescribed sequences of detectors and count intervals, both the MDAs and the variation of MDA with position on the belt might be reduced.

To derive analysis algorithms, we must adopt a coordinate system that is fixed relative to the detector array. Figure 20 shows the arrangement of the detector array and also the chosen coordinate system. As indicated, the origin is the distance of two detector diameters from the front of detector No. 1, with the x axis across the belt and the y axis along the belt in the directional senses shown. The origin is so placed because a point source more than 2.5 diameters from the center of the detector has a very small probability of detection relative to a source that is directly under the detector's center. In computing MDAs, we specify the initial position of the point source x_0, y_0 at the beginning of the first significant counting interval.

At this time, we use a belt speed of 0.5 in. per second (1.27 cm per second) so that the belt travels one detector diameter, or 5 in., in 10 s, which is the count interval that we now use. Because the detectors in the four rows are spaced at one-diameter intervals, the variation of the MDA with initial position is a function that has a regular periodic behavior. We, therefore, need to calculate the MDA for only initial positions in the ranges of $0 <= x_0 <=$ W/2 and $0 <= y_0 <=$ D/2 , where W is the width of the layer of paper and D is the detector diameter. From initial positions in the range of $0 <= y_0 <=$ D/2, a particle advances during eight counting intervals to positions where the detection probability is again small enough to have negligible influence on the magnitude of the calculated MDAs. We, therefore, consider detected counts during only eight consecutive count intervals from each of the six detectors. Figure 20 also shows the trajectory through the system of a point source whose initial position is $x_0 = 3$ and $y_0 = 2.5$, indicating the line segments traversed during the eight counting intervals.

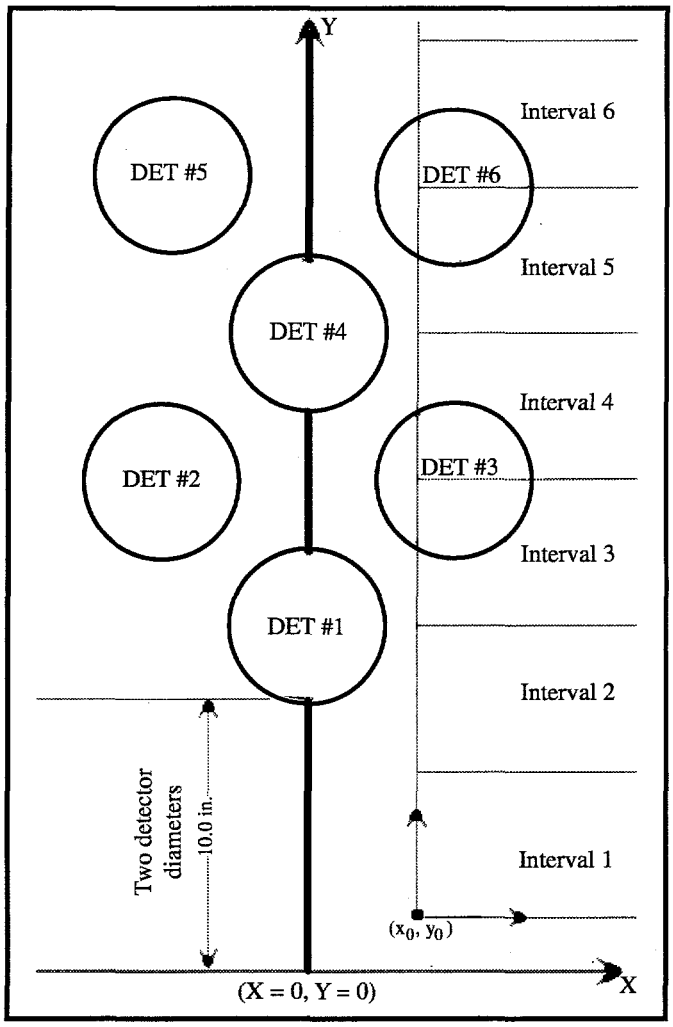

Fig. 20. Again, the geometrical arrangement of the six 5-in.-diam phoswich detectors in the present WAND system, with the selected coordinate system superposed upon it. Additionally, a sample trajectory of a radioactive particle through the system is shown with the path lengths included in the six count intervals considered.

In the calculation of MDAs, we shall make use of a number of subscripted variables, such as $C_{i,j}$, where i specifies the detector and j specifies the counting interval. The ranges for the subscripts will therefore be $1 <= i <= 6$ and $1 <= j <= 8$.

Being now fully prepared, we will discuss the independent detector analysis method in detail. Central to the independent detector analysis method (as well as to the prescribed sequence scheme) is the detector efficiency as a function of horizontal distance from the detector center E(r). Clearly, this efficiency is also a function of the vertical distance of the source below the plane of the detector face, but we simplify by assuming that the vertical distance is fixed and need not be included in the notation.

Where well-documented point sources with appropriate gamma rays are available, we use carefully measured full-energy efficiencies. For example, using a 1.155-μCi point source of ^{241}Am, we measured the efficiency at 0.5-in. intervals across a linear 15-in. interval centered on the detector face. We measured additional points at greater intervals out to 15 in. from the detector center. For distances between the measured points, we could either have fit an analytic function to the data or simply interpolated along straight line segments between successive points. Either method is adequately accurate for our needs. The more simple interpolation method is perhaps preferable because it is difficult to find an appropriate analytic function to accurately fit the measured points (in some cases even a ninth-order polynomial is not good enough). Figure 21 shows the efficiency curve for the sodium iodide response to the ^{241}Am 60-keV gamma ray at a vertical distance of 2.0 in. from the phoswich face. The data are highly precise, and they obviously form a smooth curve; in this case, a ninth-order polynomial provides an adequate fit out to r = 7.5 in. Beyond r = 7.5 in., we have always used interpolation. In Fig. 22, a logarithmic vertical scale shows the efficiency curve of Fig. 21 out to r = 15 in., thereby illustrating why the interpolation method is adequate for distances beyond r = 7.5 in. When measured curves are not available for required energies, we use interpolation between measured sets of data. We feel that this can be done with adequate accuracy.

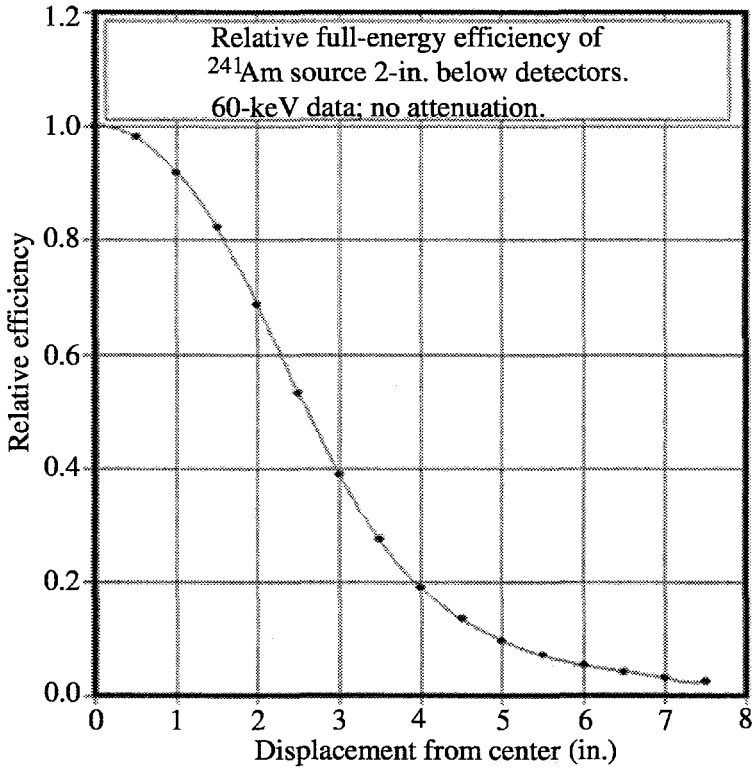

Fig. 21. The efficiency curve for the NaI response to the ^{241}Am 60-keV gamma ray at a vertical distance of 2.0 in. from the phoswich face as a function of lateral displacement (out to 7.5 in.) from the center of the detector.

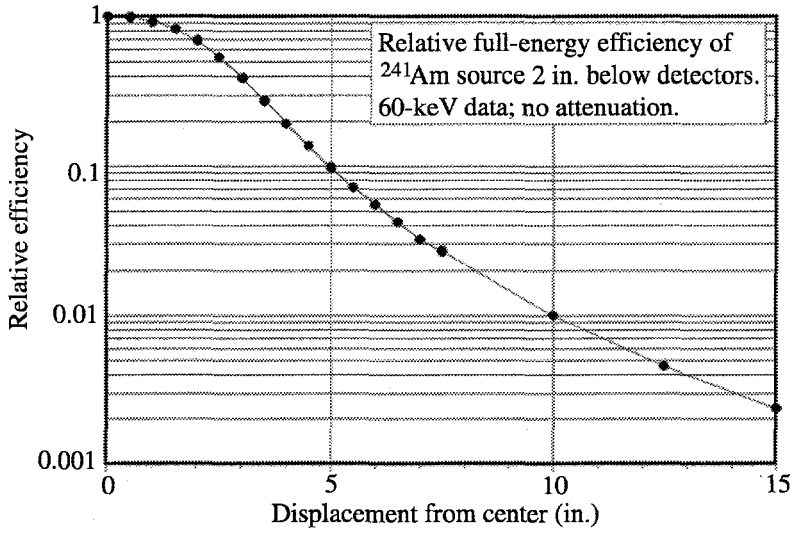

Fig. 22. The same efficiency curve shown in Fig. 21, but with logarithmic vertical scale and with displacements to 15 in. It is shown to validate the use of the interpolation scheme to obtain efficiencies in the 7.5- to 15.0-in. displacement range.

The E(r) function is always normalized so that E(0) = 1.0 and is always used in conjunction with AE_0, which, for the energy being considered, is the absolute efficiency of a point source under the center of the detector at the vertical distance being considered. To calculate the MDA, we first calculate the detection probabilities $DP_{i,j}$ for each detector during each of the eight counting intervals included. Mathematically, we define DP by

$$DP = \int E(r)\, d\ell \Big/ \int d\ell \,, \tag{1}$$

where r is the horizontal distance from the detector center to the line element dl. The integrals are along the line segments traversed by the particle with the initial position x_0, y_0 during the count intervals considered. Though E(r) can be an analytic function, we find it easier to evaluate Eq. 1 by numeric integration, which can be done quickly and with more than adequate accuracy. Note that the definition of Eq. 1 says that DP is the ratio during the count interval of the average detection probability for a source moving along the particular line segment to the detection probability of the identical source motionless at $r = 0$. Thus, in all cases $DP_{i,j} < 1$.

In actuality, for a selected energy ROI, the average background count per counting interval will vary somewhat from detector to detector, though the averages are within a few percent of one another. In order to simplify our MDA calculations a little, we make the reasonable assumption that the average background count per interval is the same for all six detectors, and we denote that average by BC_{av}.

We next select the nominal overall false-alarm probability per counting interval α. The nominal false-alarm probability for the individual detectors is taken to be $\alpha_d = \alpha/6$. Though not quite correct, it is a very good approximation for $\alpha << 1$.

Next, using the Poisson probability distribution, we use α_d and BC_{av} to find the LC, which is, of course, defined as that integer count for which $P(>= LC, BC_{av})$ is closest to α_d. Remember that in our notation (see Appendix B), $P(n, n_{av})$ is the probability of detecting n events when the average number of detected events is n_{av}. The probability is best computed from the relationship $P(>=LC, BC_{av}) = 1 - P(<LC, BC_{av})$. The expression $P(<LC, BC_{av})$ is, of course, the sum from $n = 0$ to $n = (LC-1)$ of $P(n, BC_{av})$. The upward recursion relation given in Appendix B is useful in computing the probabilities, because it allows for the computation of larger values of n without computing high powers of BC_{av} and the factorials of large numbers.

Next, we must find the average number of emitted photons per counting interval EP that will result in the average detected source count SC, which when added to BC_{av}, gives the total actual observed average count AC that produces the probability β of going undetected by every detector during any counting interval as the source passes through the system. Again, we cannot write an analytic function for EP, but must use an iterative numeric computation scheme. In the procedure that we adopted, we first assume that $EP = 10$ and, then, calculate the probability of failing to detect FP. If $FP > \beta$, we increment EP by 10 and repeat, and so on, until $FP <= \beta$. If $FP = \beta$ we have the desired EP. If $FP < \beta$, we decrement by 10 and start over using an increment of 1, then an increment of 0.1, and so on until we stop with an increment of 0.001. At this point, we have determined EP to three decimal places, which is sufficient for the purpose.

For each value of EP that we test, we must find the total actual observed count, given by $AC_{i,j} = SC_{i,j} + BC_{av}$. For each of the 48 detector/interval combinations, we then find the failure-to-detect probability $f_{i,j}$, again using BC_{av} and the previously computed LC with the Poisson distribution. The overall probability for failure to detect in any of the detector/interval combinations is equal to the product of all the individual $f_{i,j}$. Formally then,

$$FDP = \prod_{i=1}^{6} \prod_{j=1}^{8} f_{i,j} \quad . \tag{2}$$

Finally, the MDA is given by

$$MDA = EP/(F * T) \quad , \tag{3}$$

where T is the count interval in seconds and F is the emission probability for the gamma ray or x-ray being considered. We have written a code in Microsoft Quick Basic that, for a given set of initial conditions and for the chosen initial position, computes the MDA in a few

seconds on an obsolescent PC. We also have a second code which computes the MDA at 0.5-in. intervals for $0 <= x_0 <= 6$ and $0 <= y_0 <= 2.5$. We use this code, which takes ~15 m to execute on the same old PC, to study the variation of the MDA relative to position on the belt. With a faster PC, the computation time would be much less; however, even the current fairly lengthy calculation times are only mildly inconvenient because the MDA calculations are done off-line.

Now let us describe the prescribed sequence procedure. In Figs. 20 and 10 it is intuitively obvious that point sources for which $x_0 = D/2$ (in the current WAND system $D/2 = 2.5$ in.) and those at the edge of the layer of paper (for which $x_0 = 6.0$ in. in the present system) will have higher MDAs than sources with other x_0 values. It is also intuitively obvious that if we sum an appropriate sequence of detector/interval count values—namely, those which would successively receive maximum counts as the source traveled along the $x_0 = 2.5$-in. lines—we would favor those point sources and perhaps reduce the spatial variation in the MDA. With insufficient time for extensive study, we tried the following i, j sequence (i indicating the detector number, and j the interval number) of 12 combinations: 1, 2; 1, 3; 2, 3; 2, 4; 3, 3; 3, 4; 4, 4; 4, 5; 5, 5; 5, 6; 6, 5; and 6, 6.

We first formed the sum SDP of the $DP_{i,j}$ over the sequence. The $DP_{i,j}$ were identical with those computed for the independent detector method. Because we were summing together 12 of the 48 total counts, the average background was 12 times that for a single detector for a single interval. Thus, for the prescribed sequence, we had $PSBC_{av} = 12 * BC_{av}$. There was also a finite sum of detection probabilities for the sequences starting one and two intervals before the interval of the initial position and, similarly, for the sequences starting one and two intervals after the interval of the initial position. We therefore calculated the total detection probability for the five sequences as indicated and also found the probability for failure to detect for all five sequences. Empirical testing showed that the failure-to-detect probabilities of any other sequences further removed from the initial one were so near 1.00 that it is useless to include them. Their effect on the product of probabilities was negligible. We then used an iterative procedure, just as we did with the independent detector method of analysis, to find the average number of photons emitted for each interval EP for which the product of the failure-to-detect probabilities for the five sequences equaled the selected probability β.

It turns out that the MDA values found by the prescribed sequence method do have less spatial variation than do those found by the independent detector method, and the average magnitude is ~25% less. In principle then, the prescribed sequence method is better. However, it does, have one drawback. As described in the next section, we have to deal with false alarms, which currently requires stopping the belt, backing up, and recounting the interval or sequence in which the apparent alarm occurred. In the independent detector method, the belt backs up only 10 in., the distance moved in two intervals. In the prescribed sequence method, the belt must back up the distance moved in six counting intervals, which takes more time. If, however, the better quality analysis results are worth the extra time,

then users of the WAND can choose to use the prescribed sequence method if the necessary straightforward additions to the software are written and implemented.

As mentioned at the beginning of this section, the MDAs for a uniform-surface distribution of contamination are of interest although anything even remotely approaching that situation is highly unlikely. To determine these MDAs, we must make only modest modifications to the procedures outlined above.

The normalized relative efficiency function E(r), the absolute efficiency of a point source under the center of the detector AE_0, and the known background rates in the ROI being considered are still the key items of information. If the number of emitted photons per unit area per counting interval is called EP, then the count from contamination source photons is

$$SC = EP * AE_o * \int_o^{R\,\max} E(r)\, dA \quad , \tag{4}$$

where $dA = 2 * \pi * r * dr$ and R_{max} is the maximum distance to which it is worth integrating the function. In our case, we use $R_{max} = 15$ in., because the value of E(r) is negligible beyond that. As before, it is easier to do a numerical integration. Note that it is necessary, and easy, to eliminate from the integral any areas that are beyond the 12-in.-wide band of material on the belt. There are only two values for SC, one for the four detectors nearer the edge of the belt, and one for the two detectors over the center of the belt. This simplifies the computations considerably.

The LC is computed just as before. Then (and also as before), a numerical search finds the value of EP which produces the assumed failure-to-detect probability β. There are two ways of approaching this. The first is to assume that every detector is independent. For the two values of SC, we calculate the two failure-to-detect values, FP_1 and FP_2. The overall failure to detect FTD = $FP_1^4 * FP_2^2$. The value of EP that makes $FTD = \beta$ is the MDA, expressed in units of emitted photons per unit area per counting interval. In the computations, of course, it is the average background count per counting interval BC_{av} *for a single detector* that is used. This is entirely analogous to the independent detector computations for single particle sources.

Obviously, for continuous uniform distributions of contaminations there is nothing similar to the prescribed sequence method for single particles; nor is there any variation of MDA with respect to position. And, if we assume an unending stream of uniform surface contamination, there is no dependence on belt speed. The MDA will depend only on the counting interval and the background rates.

There is, however, a better way to handle the count data than that just described. The properties of the Poisson distribution suggest that we might get better results if we consider the six detectors to be a group. That is, for purposes of calculating LC, we consider the average background to be $6 * BC_{av}$; for calculating failure-to-detect probabilities, we add

together the actual counts in all the detectors. The MDA values that we calculate by grouping the data are about 61% of those found when we let each detector be independent; thus, grouping is clearly the better way to handle the count data. The values found by this method are cited in the discussion of permitted contamination limits in the Introduction section of this report.

4. Dealing with False Alarms. In order to reduce the MDA values as much as is reasonable, the WAND system uses a finite, though low, nominal false-detection probability, namely 0.001 per ROI per detector per counting interval. Because there are six detectors and four regions of interest being tested per detector, the probability of having a false alarm is ~0.024 per counting interval. This translates to a false alarm approximately every seven minutes of operation. Because WAND is confirming that the paper known to be clean, with a high degree of confidence, really is clean, there will be very few, if any, real detections of contaminant activity. The question then is how to treat the rather numerous false alarms. We, of course, want to demonstrate that they really are just false alarms.

The adopted procedure consists of stopping the belt whenever the data analysis indicates that the LC has been equaled or exceeded in some regions of interest, backing up to the beginning of the spatial increment in which the offending count occurred, and recounting. We add the original count data to the data from the second count and apply statistical tests to the combined counts. Thus far, we have only done the obvious. The important thing is how we treat the combined data.

For the WAND system, the MDA values quoted in the Introduction and in Section IV, System Performance, assume the 0.05 failure-to-detect probability. We wish to maintain both the MDA value and the 0.05 failure-to-detect probability which, fortunately, makes the false-alarm probability in the reanalysis of the combined data become very small. The following is a detailed explanation. If the MDA activity remains constant, then the average total count from the MDA plus background doubles when the counting interval doubles. This means that the original LD, which is that sum, is doubled. We calculate the Poisson distribution corresponding to 2 * LD and then find the count for LC' for which the probability of observing values less than LC' is closest to, though less than, 0.05. The average background count also doubles in the combined data. When we calculate the Poisson distribution for double the average background count and determine what the probability is of observing values equal to or greater than the LC', we find that the probability is much less than the original nominal false-alarm probability of 0.001.

An example will help to indicate the degree to which the false-alarm probability is reduced in the analysis of the combined count. If we assume a nominal false-detection probability of $\alpha = 0.001$, a failure-to-detect probability of $\beta = 0.05$, and an average background count of $BC_{av} = 1.0$, then LC = 6 with an actual false-detection probability of 0.000594, and the LD = 10.514. In a double-length count, we would have the LD = 21.028. In the Poisson distribution, for an average count of 21.028, the probability of observing < 14 is 0.0428.

Now, in the double-length count, the average background count is 2.00. In the Poisson distribution, for an average count of 2.00, the probability that the count will be ≥ 14 is only 2.93×10^{-8}. The probability of declaring clean paper to be contaminated is therefore greatly reduced. In fact, this probability implies that we would get a false alarm on the recount only about once every 500,000 days, a number that we would be happy to accept.

However, according to the limited data available as of June 1997, WAND is getting a false alarm on recount once or twice a day. It appears that the background count rate has a non-Poisson component in which rather large bursts of counts occur—perhaps a few times a day—putting abnormally large numbers of counts into a single counting interval. Recounting does not cure the problem because the number of counts in the first interval is so large that the double-length count is still above the modified LC'. Such non-Poisson bursts could come from cosmic-ray interactions or from malfunctioning equipment. We have not yet had time to determine the exact reason, though we hope to do so. Until then, at worst, the result is that once or twice a day a kilogram or two of paper is unnecessarily sent to the contaminated waste dump.

A strategy for dealing with these episodes would be to throw out the count when it is very high in a single counting interval (real contaminations would put extra counts into at least two consecutive intervals) and then to reexamine the region with a double-length count. This would be honest and would almost eliminate the problem of storing clean waste in the contaminated waste dump.

5. Software Implementation of Methods and Algorithms. We designed the custom WAND software to automate the waste-screening process. The software automatically controls the shredder and conveyor operations and collects and analyzes all data in real-time. The main user operations are background collection, assay of waste material, and quality assurance (QA) system checking.

The WAND analysis is based on the count rates in 24 separate regions of interest. These regions are set at the discretion of the system operator, based on the expected radioisotopes in the waste stream. The current configuration consists of four regions in each of the six phoswich detectors. The developers can easily expand the number of regions of interest to be analyzed to cover a broad range of isotopes, though that may be too much to expect of routine users.

In the background run, we collect a spectrum over a period of several hours or more. We typically perform this measurement during the night before we operate the instruments. At the completion of the background run, we calculate the integral counts in each region for each of the designated regions of interest. Based on the count rate in the region, the assay time, and the false alarm and failure-to-detect probabilities chosen by the system operators, we use Poisson statistics to determine the LC, the minimum LDs, and the radiation detection alarm limit for each ROI. The LC and minimum LDs have already been defined in this report.

The radiation detection alarm limit corresponds to the LC that we obtain by keeping the LD constant, while we extend the assay time by a factor of 2. We determine these three parameters separately for each of the 24 regions of interest. We write the parameters to disk and use them in all subsequent assay operations until we collect a new background count. We also write the raw count rates from each region to disk so that we can calculate new alarm limits if the operators change the assay parameters.

When we start the assay, we initiate the conveyor motion and begin the data collection. We collect spectra in short time intervals or runs, typically 10 seconds each, or roughly the time required for a point to pass beneath one of the phoswich detectors. At the completion of a run, we move the MDA data to computer memory and immediately start another spectrum without stopping the conveyor. While the next spectrum is being collected, we analyze the previous data. We then compare the number of counts in each ROI to the LC that we calculated for that ROI from the background data. If none of the ROI integrals exceed the LC, the assay continues. If the LC is exceeded in any ROI, we stop the conveyor and move it back to the starting position of the failed run. We then make a second run on the same area. At the completion of the second run, we add the ROI integrals from the second run to the integrals from the first run and compare this data to the radiation detection alarm limit described above. If the radiation detection alarm limit is not exceeded, we assume that the failed run was due to a false alarm, and we continue the assay. If the radiation detection alarm limit is exceeded, radiation has been detected on at least one of the detectors. We immediately abort the assay run and manually divert the contaminated portion of the waste on the conveyor to a low-level-waste stream.

The QA system check provides a daily check on the operating parameters of the detection system. A ^{57}Co check source is positioned under each detector. We obtain a short spectrum from each detector, after which we determine the area, centroid, and FWHM (full width at half maximum) for the 14.4- and 122.1-keV peaks. We compare the measured values to a set of limits in a parameter file. Then, at the end of the QA check, we generate and print a QA report detailing the results.

IV. SYSTEM PERFORMANCE

A. Normal Operating Parameters

We use two methods to process cellulosic waste through the WAND system: (1) feeding shredded paper to the conveyor belt via the hopper/auger mechanism, or (2) directly feeding flat stacks of paper onto the conveyor belt. (Note that stacks are approximately 0.2 g/cm^2 thick.) We currently prefer the direct-feed method for three reasons: (1) it is less time-consuming than shredding paper, (2) we have experienced mechanical difficulties getting shredded paper to feed reliably through the hopper/auger mechanism, and (3) a lot of paper dust is generated in the shredding process. We estimate from our limited operational

experience that approximately 25% of all paper waste will require shredding in order to process through the WAND system.

The WAND system's conveyor belt, auger, and phoswich detectors all operate through an interface with the system software, while shredding and feeding paper onto the conveyor belt are performed manually. We set the conveyor belt to move at a speed of 1.27 cm/s (0.5 in./s), but it has a maximum speed of approximately 2.0 cm/s (0.8 in./s). We place all paper waste in the middle 12 in. of the 21-in.-wide conveyor belt to achieve an optimal source-to-detector geometry. We control the facility temperature at 21°C ± 2°C (70°F ± 4°F) to minimize the energy drift of the detectors during the course of a day.

The weights of typical 2-cu-ft waste boxes range from 5 to 15 kg, so we require an average processing time of 15–45 minutes per box (note that the total processing time includes all necessary documentation, bag change-outs, etc.). To function at the optimal level, the system requires two trained technicians to operate it; however, one technician can perform all of the required work in approximately 150% of the time.

B. Detailed Presentation of MDA for ^{241}Am and Its Spatial Variation

One of the most important nuclides for which the WAND system must have high sensitivity is ^{241}Am, because at LANL much waste comes from the Plutonium Facility. Therefore, there is potential plutonium contamination, and most of the plutonium waste has some associated ^{241}Am, which builds in from the decay of ^{241}Pu. Because ^{241}Am has both a 59.54-keV gamma ray that is emitted in 35.9% of decays and L x-rays that are emitted in about 37.4% of all decays, the WAND system will have a very high sensitivity for that nuclide. At LANL it is relatively easy to obtain and to use low-level ^{241}Am standards. It has therefore been possible to study and confirm the WAND system's performance in detecting ^{241}Am in considerable detail. The results are reported here as a detailed example of the system's performance.

As mentioned previously, the MDA varies somewhat with respect to the position of point sources on the belt relative to the detector array. This will be shown in detail, but first we present the maximum, average, and minimum values for two conditions. Both conditions are for point sources on the belt 2.00 in. beneath the face of the detectors, but in the first condition there is no attenuating material and in the second condition the point sources are covered with 0.2 g/cm^2 of paper (assumed to be cellulose, $C_6H_{10}O_5$). These are quite useful choices. The first case is the easily confirmed base or demonstration case, and the second is the worst case. Sources within the layer of paper are, on the average, closer to the detectors and suffer less attenuation; therefore they will have lower MDAs than the worst case.

The results are presented in Table II. In addition to the conditions specified above, the results assume a failure-to-detect probability of 0.05, a nominal false-detection probability of 0.001 per ROI (implying an overall false-detection probability of ~ 0.024 per counting interval), a belt speed of 0.5 in./s, and a counting interval of 10 s. The background count in

the 60-keV ROI is 0.2/s, and in the L x-ray ROI is 0.4/s. The efficiencies for point sources of ^{241}Am directly under the detector centers are 0.16 for the 60-keV gamma rays and 0.14 for the L x-rays. Lastly, we set the 60-keV mass attenuation coefficient for cellulose at 0.21 cm^2/g and for L x-rays (assumed to be 15 keV) at 1.3 cm^2/g.

It is clear that the MDAs based on the 60-keV gamma ray are lower than those based on the L x-rays, even though the emission probabilities are nearly the same. All the 60-keV values are less than 1 nCi, an excellent performance when based on photons with much lower abundances than the alpha emissions. For the no-attenuation cases, the difference in MDAs results from the approximately twice-as-high background rate in the lower-energy L x-ray ROI and from a slightly lower efficiency. For the 0.2-g/cm^2 case, the higher mass attenuation coefficient in the lower-energy ROI also increases the difference.

The fractional differences relative to the averages of the maximum and minimum values are significant, though they are acceptable in a waste-screening application. For the 60-keV results with 0.2 g/cm^2 of assumed cellulose for attenuation, the maximum is 36% higher than average and the minimum is 19% less than average. For the L x-ray results with 0.2 g/cm^2 of assumed cellulose for attenuation, the maximum is 55% higher than average and the minimum is 25% lower than average.

Table II. WAND System MDAs for ^{241}Am under Present Normal Operating Conditions Using Independent Detector Analysis

	60-keV gamma rays (disintegrations per second)		**~ 15-keV L x-rays (disintegrations per second)**	
	No. Atten.	0.2 g/cm^2	No Atten.	0.2 g/cm^2
maximum	26.20	28.40	40.60	66.00
average	19.60	20.90	29.00	47.60
minimum	16.00	16.90	23.30	31.90

The prescribed sequence analysis, which is not yet implemented in the WAND system, produces significantly better results with respect to both MDA magnitudes and spatial variation. Table III gives the results for the prescribed sequence analysis under the same conditions that we used to calculate the independent detector method results of Table I.

Table III. WAND System MDAs for ^{241}Am under Present Normal Operating Conditions Using Prescribed Sequence Analysis

	60-keV gamma rays (disintegrations per second)		**~ 15-keV L x-rays (disintegrations per second)**	
	No. Atten.	0.2 g/cm^2	No Atten.	0.2 g/cm^2
maximum	16.80	18.00	25.50	38.80
average	14.40	15.50	21.80	34.00
minimum	12.80	13.80	19.50	29.40

Note that the averages in Table III are about 73% as high as those in Table II and that the deviations of the maximums and minimums from average are also less. The prescribed sequence method should be more carefully investigated. The data here are the result of the first, rather intuitively obvious sequence that was tried. It is also possible that a different geometric arrangement of the detectors could reduce the spatial variation of MDAs and that some study would be in order before possible upgraded versions of the WAND system are built.

MDA might be improved by redefining it as the activity that has a 0.05 probability of simultaneously failing to detect in both the 60-keV gamma-ray and the L x-ray ROIs. When calculated, it appears that there is only a 14% decrease in MDA—useful perhaps, but not overwhelming. If, however, we maintain the 60-keV MDA value of 57.7 ^{241}Am disintegrations per second, then by using both ROIs to calculate the MDA we reduce the failure-to-detect probability to ~0.016.

Tables IV and V show in detail the spatial variation of the MDA with respect to position on the belt. The figures in the body of the tables are normalized to the average, which we set at 1.00. Thus the fractional deviations from the average are clear. Values are computed at 0.5-in. increments for $0 <= x_0 <= 6$ and for $0 <= y_0 <= 5$. Table IV presents the variation for the ^{241}Am 60-keV gamma ray with the point source on the belt 2.0 in. beneath the detectors, covered by 0.2 g/cm^2 cellulose and analyzed by the independent detector method. All other parameters are as specified above. Table V gives results using the prescribed-sequence method for conditions matching those in Table IV. As expected, the results are symmetric about the y = 2.5-in. line; symmetric about the y-axis of our coordinate system (see Fig. 20); and periodic, with a 5-in. period along the y-axis.

Table IV. MDAs Normalized to Average = 1.00 as a Function of Position

Independent Detector Analysis													
y\x	0.00	0.50	1.00	1.50	2.00	2.50	3.00	3.50	4.00	4.50	5.00	5.50	6.00
5.00	0.81	0.83	0.89	0.99	1.12	1.19	1.12	0.99	0.89	0.83	0.81	0.83	0.90
4.50	0.82	0.84	0.90	1.01	1.14	1.20	1.14	1.01	0.90	0.84	0.82	0.84	0.91
4.00	0.85	0.87	0.93	1.04	1.17	1.24	1.17	1.04	0.93	0.87	0.85	0.87	0.94
3.50	0.89	0.91	0.97	1.08	1.22	1.29	1.22	1.09	0.97	0.91	0.89	0.91	0.98
3.00	0.92	0.94	1.01	1.12	1.27	1.34	1.27	1.12	1.01	0.94	0.92	0.94	1.02
2.50	0.93	0.95	1.02	1.14	1.29	1.36	1.29	1.14	1.02	0.95	0.93	0.96	1.03
2.00	0.92	0.94	1.01	1.12	1.27	1.34	1.27	1.12	1.01	0.94	0.92	0.94	1.02
1.50	0.89	0.91	0.97	1.08	1.22	1.29	1.22	1.09	0.97	0.91	0.89	0.91	0.98
1.00	0.85	0.87	0.93	1.04	1.17	1.24	1.17	1.04	0.93	0.87	0.85	0.87	0.94
0.50	0.82	0.84	0.90	1.01	1.14	1.20	1.14	1.01	0.90	0.84	0.82	0.84	0.91
0.00	0.81	0.83	0.89	0.99	1.12	1.19	1.12	0.99	0.89	0.83	0.81	0.83	0.90

Table V. MDAs Normalized to Average = 1.00 as a Function of Spatial Position

Prescribed Sequence Analysis													
y\x	0.00	0.50	1.00	1.50	2.00	2.50	3.00	6.50	4.00	4.50	5.00	5.50	6.00
5.00	0.89	0.90	0.93	0.97	1.01	1.03	1.02	0.99	0.97	0.96	0.97	1.02	1.11
4.50	0.89	0.90	0.93	0.97	1.01	1.03	1.02	0.99	0.97	0.96	0.97	1.02	1.12
4.00	0.90	0.91	0.94	0.98	1.02	1.04	1.03	1.01	0.98	0.97	0.99	1.03	1.13
3.50	0.92	0.93	0.95	0.99	1.04	1.05	1.05	1.02	0.99	0.98	1.00	1.05	1.15
3.00	0.93	0.94	0.96	1.01	1.05	1.07	1.06	1.03	1.01	1.00	1.01	1.06	1.16
2.50	0.93	0.94	0.97	1.01	1.05	1.07	1.06	1.04	1.01	1.00	1.02	1.07	1.17
2.00	0.93	0.94	0.96	1.01	1.05	1.07	1.06	1.03	1.01	1.00	1.01	1.06	1.16
1.50	0.92	0.93	0.95	0.99	1.04	1.05	1.05	1.02	0.99	0.98	1.00	1.05	1.15
1.00	0.90	0.91	0.94	0.98	1.02	1.04	1.03	1.01	0.98	0.97	0.99	1.03	1.13
0.50	0.89	0.90	0.93	0.97	1.01	1.03	1.02	0.99	0.97	0.96	0.97	1.02	1.12
0.00	0.89	0.90	0.93	0.97	1.01	1.03	1.02	0.99	0.97	0.96	0.97	1.02	1.11

C. Brief Presentation of MDAs for Other Nuclides

In order to calculate the MDA for a given nuclide, we must know the following: the background rate in any ROI which falls within the radiation spectrum of that nuclide; the efficiency as a function of radial distance from the detector center for the energy involved; and the probability of the detected photons being emitted in the decay of the nuclide. Measuring the efficiency functions is a significant amount of work and requires appropriate sources of the desired nuclides. In the cases of nuclides for which appropriate standards are not available, we can use other nuclides to make extrapolations from measured values, usually with adequate accuracy. Because of this rather labor-intensive situation, we have thus far (June 1997) performed careful calculations of MDAs for only two other nuclides: ^{239}Pu and ^{137}Cs.

For ^{239}Pu, the MDAs are about a factor of 10 higher than for ^{241}Am because the emission probability for the L x-rays is only 4.7% and there are no higher-energy gamma rays of comparable emission probability. For the individual analysis method, the average MDA is 230 dps for a point source on the bare belt and 340 dps when 0.2g/cm^2 of paper are put over the source.

For ^{137}Cs, there are two photons that are useful; the 661.6-keV gamma ray that is emitted 85% of the time and the 30-keV K x-rays of barium that are emitted 7.8% of the time. Based on the individual detector analysis, the 661.6-keV gamma ray gives an MDA of 51.8 dps, and the 30-keV x-rays give an MDA of 92.5 dps. As expected, the 661.6-keV value comes from interactions in the cesium iodide crystal, and the 30-keV value comes from interactions in the sodium iodide crystal.

V. OPERATING PROCEDURES AND QUALITY ASSURANCE

We have successfully developed and used procedures for operating and calibrating the WAND system in a brief pilot demonstration of the process. We updated the procedures immediately following the pilot project to reflect the lessons learned. The operating procedure stipulates that when radioactivity greater than background levels is detected in any portion of the waste, all the waste in the container is considered to be radioactive by association. This conservative approach is practical because very few containers are expected to have added radioactivity. However, if desired, the portion of waste found to contain added radioactivity could easily be segregated from the clean portion of the waste and disposed of separately.

The calibration procedure includes sections on performing energy and efficiency calibrations of the phoswich detectors as well as a section on gating the sodium iodide and cesium iodide pulses with the WAND system multiplexer. To control excessive energy drift, we perform calibration checks daily when the system is operational. Absolute-efficiency determinations for the L x-ray and the 59.5-keV regions of interest are performed annually with an NIST-traceable, ^{241}Am source. We initially determined linear fitting equations for the energy calibration of each cesium iodide spectrum, and these will be reevaluated annually. Gating sodium iodide and cesium iodide pulses with the system multiplexer is a one-time procedure that we perform when the detectors are initially brought on-line.

The phoswich detectors are energy calibrated using the 14.4- and 122.1-keV peaks produced by ^{57}Co sources in the sodium iodide portion of the spectra. The cesium iodide energy calibration is independent of the sodium iodide calibration and is primarily a function of the cesium iodide crystal's light output relative to that of the associated sodium iodide crystal. Therefore, while all sodium iodide spectra are energy calibrated the same, each cesium iodide spectrum has a unique energy calibration dependent on its relative light output. The calibration of the sodium iodide crystals allows the system to detect low-energy photon radiations and beta particles up to approximately 800 keV in energy, while the resulting cesium iodide calibrations allow for the detection of photons up to approximately 1800 keV ($\pm$ 200 keV). Currently, only one ROI in the cesium iodide spectrum is set to detect the 661.7-keV gamma-ray from ^{137}Cs; we would need to set additional regions of interest to detect other radionuclides with high-energy, gamma-ray emissions.

To ensure that the WAND system is functioning acceptably, we implemented a thorough, long-term quality assurance (QA) program and a daily quality control (QC) process. Three key elements of the QA program that ensure the long-term success of the WAND measurement system are as follows: (1) we directly incorporate into the WAND system procedures those processes that are needed to identify, report, and correct conditions adverse to the proper functioning of the WAND system; (2) we perform corrective actions when we observe long-term trending of data that will affect the proper functioning of the WAND system; and (3) we update procedures to directly reflect lessons learned from

operational experience and distribute these updates to all staff members that may feel the impact of the changes.

There are three elements of the daily QC process: (1) an evaluation of background rates, (2) a comprehensive calibration check, and (3) a QC spike measurement. All off-normal system responses discovered during the daily QC process must be investigated and resolved by the facility supervisor before we allow the system to operate. Waste verified as clean is not released to the clean-waste dumpster until the daily QC process is successfully completed both at the start of the day of the actual measurement and then again on the following work day.

In the first step in the daily QC process, we review and evaluate background rates in the four regions of interest from the previous evening's background count. A primary concern is that background rates might exceed expectations, thus increasing detection limits. Higher-than-normal background rates could be an indication of contamination on the conveyor belt, a change in the energy calibration of a detector, or an unexpected change in the shielding configuration around the detectors. We consider background rates to be acceptable if they are within 3σ of the mean rate for each ROI. If we determine that any background rates are higher than the 3σ acceptance criteria, we perform a quick evaluation to determine the reason behind the increased rate. We continue operations when the cause of the increased rate is found and corrected or is otherwise determined to be insignificant. We track and evaluate background rates weekly to determine any trending of the data.

Following the evaluation of background rates, we perform a calibration check on all six phoswich detectors. Six ^{57}Co sources, with a nominal activity of 0.5 μCi each, are guided beneath the WAND detectors in a fixed geometry for a 100-s calibration check. ^{57}Co produces three distinct photopeaks in the phoswich detector: a 14.4-keV x-ray in the sodium iodide crystal and a 122.1-keV gamma-ray peak that appears in both the sodium iodide and cesium iodine crystals in comparable amounts. The software-driven calibration check evaluates each peak's centroid channel number, FWHM, and net area for each of the six phoswich detectors. All measurement results must meet prescribed acceptance criteria before operations may proceed. Because a total of 54 parameters must meet acceptance criteria, we set acceptance ranges liberally enough so that random statistical fluctuations do not cause the system to constantly fail the calibration checks. However, adjustments of the fine gain on one or two detectors are commonly required, especially when the temperature in the facility changes by a few degrees. Table VI presents the measurement parameters and acceptance criteria for the daily WAND system calibration check.

Table VI. Acceptance Criteria for WAND System Daily Calibration Check

Measurement parameter	14.4-keV peak in NaI crystal	122.1-keV peak in NaI crystal	122.1-keV peak in CsI crystal
Peak Centroid	± 0.75 channels	± 1.5 channels	± 1.5 channels
FWHM	± 1.5 keV	± 2.0 keV	± 2.0 keV
Net Area	± 5.0 percent	± 5.0 percent	± 5.0 percent

The facility technician keeps a record anytime the fine gain on a detector is adjusted so the facility supervisor can determine if a detector or associated electronics are developing any problems. On a weekly basis, we track and review the net peak areas measured during the daily calibration check to determine if long-term trending of data is occurring.

In the final step in the daily QC system check, we measure a QC spike standard in the normal operational mode. We place standards with activities nominally greater than the system MDA on the conveyor belt, and we start the system as if normal operations had commenced. The QC spike check is complete when the system software stops the conveyor belt and produces a "Radiation Detected" signal on the screen. Five different QC spike standards are rotated in use during the course of a week: ^{239}Pu, ^{241}Am, ^{238}U, ^{137}Cs, and ^{36}Cl. We do not consider blind spikes of deliberately contaminated paper waste to be practical because of the potential for contamination of system components. Nor do we consider QC checks with blank standards to be practical because we expect virtually 100% of the waste processed by the WAND system to be uncontaminated (i.e., effectively "blanks").

VI. REFERENCES

1. "Radioactive Waste Management," Department of Energy Order 5820.2 (September 26, 1988).

2. "Radiation Protection of the Public and the Environment," Department of Energy Order 5400.5 (February 8, 1990).

3. LANL Radiological Control Manual, Los Alamos National Laboratory internal electronic document (December 23, 1994).

4. L. A. Currie, "Limits for Qualitative Detection and Quantitative Determination," *Anal. Chem.* **40**, (3), 587 (1968).

5. J. C. Lochamy, "The Minimum Detectable Activity Concept," (Presented at the National Bureau of Standards 75th Anniversary Symposium), EGG/ORTEC Systems Application Studies PSD No. 17, (September 1981).

APPENDIX A

PROPOSED FREE-RELEASE VERIFICATION LIMITS FOR TWO UNREGULATED LANL WASTE STREAMS*

Document Number: TD-54G-006

Authors: Diana Hollis,
Dave Jamriska,
Don Dry, and
Mark Waterman

*This is a Los Alamos National Laboratory internal Technical Area 54 document.

PROPOSED FREE-RELEASE VERIFICATION LIMITS FOR TWO UNREGULATED LANL WASTE STREAMS

1. INTRODUCTION

The Los Alamos National Laboratory (LANL) has implemented a pilot program called *Green is Clean* to examine the feasibility of free releasing certain wastes that, although generated in Radiological Controlled Areas (RCAs), are known to be free of regulated contaminants including radioactivity. *Green is Clean* is a pollution-prevention/waste minimization program: If *Green is Clean* materials are recycled, waste has been prevented; if waste is diverted from the LANL low-level radioactive waste (LLW) disposal facility, LLW waste has been minimized.

The wastes under consideration for Phase I of *Green is Clean* are known by the generator to be uncontaminated, low-density materials (e.g., paper, thin plastic, cardboard, etc.). In such low-density materials, it is possible to measure radioactivity at very low levels, even nonpenetrating alpha particles. These two things- documented knowledge of the waste-generating and segregation process, and the ability to detect minute quantities of potential contamination, provide defense-in-depth for the *Green is Clean* program.

Radiation detection instruments used to verify *Green is Clean* waste must be capable of detecting radioactivity at levels that will ensure protection of human health and the environment now and in the future. To determine detection limits that provide this assurance, a dose assessment was performed. The dose assessment was used to calculate concentrations of radioactivity that could, should the segregation step fail, inadvertently be present and not detected in *Green is Clean* waste without any risk to human health or the environment.

Under the *Green is Clean* program, LANL will release waste for disposal at the county landfill that are not believed to contain radioactive material. To verify that the waste is safe for sanitary disposal, LANL is implementing a rigorous measurement program to ensure that no waste found to contain detectable levels of residual radioactive material will be released. This report discusses the approach and results of the dose assessment performed to define detection limits that must be achieved by instruments used to verify *Green is Clean* waste released for disposal at the county landfill. Two verification systems have been qualified as part of the pilot program; both are capable of detecting between 10 and 10,000 times below the 1-mrem limits for identified radionuclides.

2. MODELING METHODOLOGY

The methodology used in the dose assessment to define detection limits for instruments used to verify *Green is Clean* waste follows guidance provided by the Department of Energy.[1] That guidance states that the limits should be based on an assessment that demonstrates that

1. release of the material will not cause a maximum individual dose to a member of the public in excess of 1 mrem in a year or a collective dose of more than 10 person-rem in a year, and doses are as low as reasonably achievable (i.e., ALARA) ; and
2. ground water will be protected.

The first of these objectives was accomplished by means of a dose assessment that considers all significant pathways of exposure for likely or reasonably expected uses of the Los Alamos County landfill during operations and after closure. The second objective is

demonstrated by application of a detailed groundwater transport model developed for another similar site.

The general assumptions invoked in the dose assessment analyses are that:

- 500 cubic meters of *Green is Clean* waste is disposed of at the Los Alamos County landfill in one year;
- *Green is Clean* waste is disposed of with 150,000 cubic meters sanitary waste[2];
- *Green is Clean* waste contains unit concentrations (i.e., 1 pCi/g) of the radionuclides listed in Table 1, which were identified by generators as being present in the RCAs in the pilot facilities.

Table 1. Radioisotopes present in pilot facility radiological controlled areas.

Radioisotope	Half-Life
Be-7	54 days
Na-22	2.6 years
Al-26	740,000 years
Si-32	100 years
Ti-44	52 years
V-48	16 days
V-49	330 days
Cr-51	28 days
Mn-54	303 days
Fe-55	2.6 years
Fe-59	46 days
Co-56	77 days
Co-57	270 days
Co-58	71 days
Co-60	5.2 years
Ni-59	80,000 years
Ni-63	92 years
Zn-65	245 days
Ge-68	275 days
As-73	80 days
As-74	18 days
Se-75	120 days
Sr-82	25 days
Se-85	64 days
Sr-90	28 years
Rb-83	100 days
Rb-84	33 days
Rb-86	19 days
Zr-88	85 days
Zr-95	65 days
Nb-91	700 years
Nb-91m	64 days
Nb-92	350 years
Nb-93	16 years
Nb-94	20,000 years
Nb-95	35 days
Tc-95m	61 days

Tc-97	2,600,000 years
Tc-98	4,200,000 years
Tc-99	212,000 years
Rh-101	3 years
Rh-102	206 days
Rh-102m	2.9 years
Ag-108m	5 years
Ag-110m	255 days
Cd-109	453 days
Cd-113m	14 years
Sn-113	115 days
La-137	60,000 years
Gd-150	2,100,000 years
Eu-150	5 years
Eu-152	13 years
Eu-154	8.8 years
Dy-154	10 years
Tb-157	150 years
Tb-158	1,200 years
Hf-172	5 years
Hf-178m	4.3 seconds
Lu-173	1.4 years
Lu-174	3.6 years
Lu-174m	140 days
Ta-179	600 days
Ta-182	115 days
Re-183	71 days
Re-184	38 days
Re-184m	169 days
Os-185	94 days
Hg-194	2 years
Pb-202	300,000 years
Bi-207	30 years
Bi-208	368,000 years
Po-209	103 years
U-234	247,000 years
U-235	710,000,000 years
U-238	4,510,000,000 years
Np-237	2,140,000 years
Pu-238	86 years
Pu-239	24,390 years
Pu-240	6,580 years
Pu-241	13 years
Pu-242	379,000 years
Am-241	433 years
Am-243	7,590 years

Waste disposed of at the Los Alamos County landfill is placed in 3-meter lifts, separated by 15 centimeters of clean soil between adjacent lifts.[2] The *Green is Clean* waste encountered by the disposal facility worker and a future resident contains unit concentrations of radioactivity (prior to any radioactive decay), mixed with uncontaminated waste and clean

backfill. For the groundwater protection analysis, the total inventory of radionuclides present in the 500 cubic meters of *Green is Clean* waste is assumed to be homogeneously distributed throughout the disposal unit volume.

2.1 Dose Assessment

The dose assessment summarized here and detailed in Appendix A determines how much radioactivity *inadvertently present* and *undetected* in *Green is Clean* waste could be tolerated within the following dose constraints:

- 1 mrem annual dose limit to a worker at the Los Alamos county landfill during the operational period,
- 1 mrem annual dose limit to a member of the public during the operational and post-closure periods,
- 10 person-rem annual collective population dose during the operational and post-closure periods, and
- 100 mrem annual dose limit to a future site resident during a 1,000-year post-closure period.

The 1-mrem dose constaint is assumed to implicitly address the ALARA specification previously mentioned. The approach is to calculate the effect (i.e., dose to a worker, member of the public, or future site resident) resulting from unit mass-concentrations of radionuclides (i.e., 1 pCi/g), and then to scale the result by the ratio of the applicable dose constraint to the calculated dose. The most restrictive (i.e., the lowest) mass-concentrations calculated in this exercise are proposed limits (in pCi/g) that detection systems used to verify *Green is Clean* waste for free-release must be capable of detecting.

A thorough discussion of the dose assessment summarized in this section is found in *Radionuclide Concentration Limits for the Disposal of Waste with Low Levels of Radioactivity at the Los Alamos County Landfill.*[3]

2.1.1 Worker Dose

During operations, doses to workers who may come in contact with the waste are assumed to bound offsite public doses. Workers include individuals transporting waste to the landfill and individuals disposing of waste at the landfill. Of these, the potential exposures were considered to be largest to a landfill worker. Exposures to a transporter should be smaller because the time spent in contact with the waste is less, the distance from the waste is greater, and there is shielding (i.e., the truck body) between the waste and the transporter.

The waste with which the disposal facility employee works consists of *Green is Clean* waste, diluted with uncontaminated trash and backfill. This dilution reduces the radionuclide concentrations in the disposal unit to 0.32 percent of the assumed 1-pCi/g concentration, prior to any radioactive decay. Based on input from landfill employees, the operator of the bulldozer at the landfill was identified as the maximally exposed worker.[4] The bulldozer operator is assumed to work on a partially filled, uncovered disposal unit for 8 hours per day and 2,000 hours per year. Over the period of one year, 500 m3 of *Green is Clean* waste is assumed to be disposed of by the worker. The worker is assumed to be in direct contact with the waste for 2 hours a day, and in a bulldozer for 6 hours a day. He is exposed to direct radiation from waste, and to airborne radioactivity in the form of dust. Internal exposures occur due to the inhalation of suspended contamination and from the ingestion of small amounts of soil.

2.1.2 Public Dose

The potential for exposures of members of the public depend on the amount of contaminated material that could be transported away from the landfill in air and water. During the operational period, it was assumed that worker doses would be greater than public doses. The methodology used to evaluate doses to members of the public during the post-closure period is borrowed from the *Performance Assessment and Composite Analysis for Los Alamos National Laboratory Material Disposal Area G.*[5]

The performance assessment is a technically rigorous evaluation of the potential for future members of the public to receive radiological doses due to unplanned releases of radioactivity associated with waste disposed of at a LANL Technical Area (TA)-54, Area G. The performance assessment demonstrates that the natural characteristics of the TA-54, Area G site effectively eliminate the possibility of offsite exposures to radioactivity. The Los Alamos County landfill is situated and operated much like the disposal facility at TA-54, Area G. This fact allows the detailed model developed for the Area G performance assessment to be applied to the Los Alamos County landfill, provided that differences between the two facilities that impact dose projections are accounted for. Such difference include local hydrogeology, waste disposal operations, disposal unit closure design, and institutional control period.

To evaluate potential public doses in the post-closure period after the Los Alamos County landfill is closed, capped, and controlled for a period of 30 years pursuant to regulations, release and transport of contaminants as a result of the following natural processes are considered:

- dissolution of contaminants in water percolating through the waste and transport in groundwater to the regional water-supply aquifer,
- erosion of the landfill cover and subsequent transport of exposed contaminants in air and surface water, and
- translocation of radionuclides from the disposal unit to surface soils as a result of plant and animal intrusion and transport in air and surface water, and

The groundwater pathway is discussed later in this section to demonstrate protection of groundwater. As will be described, the natural geologic and hydrologic features of the region effectively eliminate the groundwater pathway for radionuclide migration. Of the two remaining natural processes potentially leading to release of unit mass-concentrations of contamination, surface erosion has a negligible effect. The rate of erosion of a simple landfill cover comprised of compacted tuff, topsoil, and native vegetation is 4×10^{-8} meters per year. At this rate, the 0.6-meter cap[6] used at the Los Alamos County landfill effectively eliminates the potential for surface contamination as a result of erosion for millions of years. Thus, the only natural process remaining for making contamination available for transport offsite is biotic translocation.

Both plants and animals can be important biological vectors in translocating contamination from below ground to the ground surface, especially over extended periods of time. The models used in the Area G performance assessment to calculate surface contamination as a result of root uptake and excavation by burrowing animals are applicable at the Los Alamos County landfill, assuming that natural ecological succession will result in similar ecosystems, with a simple correction to reflect the difference in cover thickness. The nominal cover thickness assumed for the Area G model is 1 meter. For the 1-meter thick cover, the maximum surface-contamination concentrations are generally about 7 percent of the disposal-unit concentrations.[7] Correcting by the ratio of cover, the maximum surface-contamination concentrations can be expected to be 1.1 times the original concentration of

radionuclides within the landfill. As discussed above, the nominal homogeneous distribution of radionuclides in this exercise is 0.0032 pCi/g. Thus, the maximum surface concentration would be 0.0035 pCi/g.

The public dose consequence of this surface concentration is calculated by assuming that the contamination is transported in air to a location accessible to members of the public. The offsite doses to members of the public due to atmospheric dispersion of contamination brought to the surface by plants or animals will be at most equal to and realistically several orders of magnitude less than the dose to workers exposed to roughly the same concentrations. Using standard Gaussian dispersion relationships used by the Environmental Protection Agency,[8] the concentration of contamination suspended in air above the Los Alamos County landfill will be reduced by 7 orders of magnitude over the 2-kilometer distance between the landfill and Los Alamos.[9] For this reason, the dose to the worker due to the air pathway is expected to bound the offsite dose.

2.1.3 Future Site Resident Doses

After closure of the landfill and an institutional control period of 30 years, doses are calculated for a standard "agricultural resident" scenario, wherein:[10]

- a person builds a basement home at the Los Alamos County landfill site;
- a 3-meter deep basement is excavated into disposal units containing *Green is Clean* waste;
- one-third of the exhumed material is used as backfill outside of and around the basement walls;
- two-thirds of the material is distributed over the lot on which the house is constructed; and
- vegetables and grain grown for personal consumption become contaminated by root uptake and rainsplash.

Doses are received by the agricultural resident from ingestion, inhalation, and direct radiation exposure routes. Ingestion doses are received from the consumption of contaminated vegetables and grain grown at the site. Inhalation doses result from suspension of contaminated surface soil from the excavated material spread over the resident's lot and, for some radionuclides, from radon gas entering into the individual's home. Direct radiation from exhumed waste, waste that remains buried in the disposal units, and airborne radioactivity is also considered. The agricultural resident scenario was assumed to be plausible at any time over a period of 1,000 years following the end of the 30-year institutional control period.

2.2 Groundwater Protection

The Area G performance assessment implemented a sophisticated three-dimensional computer model to simulate the flow of water and the transport of radionuclides from disposal units to the regional aquifer. The model demonstrates that the geologic and hydrologic features of the Bandelier Tuff into which the disposal units at Area G are excavated effectively eliminate the migration of radionuclides in groundwater for tens- to hundreds-of-thousands of years. By scaling for differences in the Bandelier Tuff at the Los Alamos Countly landfill and at Area G, the Area G model is applied to the Los Alamos County landfill to demonstrate groundwater protection.

Figure 1 illustrates the stratigraphy across the Pajarito Plateau in a generalized West-East cross-section. The relative location of TA-54, Area G and the Los Alamos County landfill are shown in the figure. One significant difference between the two sites is the thickness of the Bandelier Tuff. Another is the presence of Cerros del Rio basalt beneath Area G, and the absence of basalt beneath the County landfill.

The Bandelier Tuff was formed from two distinct volcanic eruptions, the lower Otowi Member (erupted about 1.6 million years ago) and the upper Tshirege Member (erupted about 1.1 million years ago). Thin ash fall layers exist at the base of both members, the Cerro Toledo Interval beneath the Tshirege Member, and the Guaje Pumice Bed beneath the Otowi Member. Both members of the Bandelier Tuff are thicker towards the west, where the volcanic centers from which the deposits originated are located; this is indicated in Figure 1. The Tshirege Member is a compound cooling unit described by several subunits. At the Los Alamos County landfill, the Tshirege Member is quite thick and includes Units 3, 2, and 1, while at Area G, it is thinner and includes only Units 2 and 1. At both sites, Unit 1 is further partitioned into a "vitrified" layer (Unit 1v) and a "glassy" layer (Unit 1vg).

Figure 1. Generalized stratigraphy of the Pajarito Plateau, showing relative location of TA-54 and the County Landfill

To ensure that the TA-54, Area G groundwater transport model can be applied to the Los Alamos County landfill site, the hydrological and geological properties of the two sites were compared and shown to match closely.[11] With respect to model application, the significant difference between the two sites is the thickness of the Bandelier Tuff. The data in Table 2 compare the thicknesses of each section of the tuff at the two sites. While the Area G mesa is capped with Unit 2 of the Tshirege Member and the County landfill mesa is capped with Unit 3, the important hydrologic and mineralogic properties of Unit 3 that affect groundwater transport are within the range of Units 2 and Unit 1.

Table 2. Thickness of Subunits of the Tshirege Member of the Bandelier Tuff

Bandelier Tuff Section	Thickness (m)	
	Area G	County LF
Unit 3	n/a	30
Unit 2	20	21
Unit 1v	20	20
Unit 1g	13	21
Cerro Toledo	4	9
Otowi	30	85
Guaje	7	8

The depth to the regional aquifer is about 300 meters beneath Area G, and about 400 meters beneath the County landfill. About 100 meters of this distance is composed of Bandelier Tuff beneath Area G, with the remaining 200 meters being composed of Cerros del Rio basalt. In contrast, essentially the entire thickness of unsaturated rock beneath the County landfill is Bandelier Tuff. While data are available to characterize the flow and transport properties of the Bandelier Tuff, very few data are available describing the Cerros del Rio basalt. As a result, transport was calculated only through the upper well-characterized portion of the stratigraphy comprising the Bandelier Tuff, while the basalt was essentially ignored.

The Area G model assumes that groundwater moves at a constant rate of 5 mm/yr through the Bandelier Tuff. This is an extremely conservative (i.e., high) rate given the fact that several lines of field data suggest that almost no liquid water moves through the mesa at the observed moisture contents.[12,13,14] Moisture content in the Bandelier Tuff constructing

mesas in the Los Alamos region is generally less than 5 percent by volume. Laboratory measurements show that water does not move through the tuff unless present in greater amounts. In lesser amounts, water is held within the pore space of the tuff by capillary forces, where it resides until liquid volume increases, or perhaps until it is evaporated. Several recent independent analyses suggest that evaporation occurs deep within the mesa along cooling joints and surge beds at the base of Unit 2 of the Tshirege Member of the Bandelier Tuff. This very dry zone is apparent in mesas across the LANL complex, not only at Area G. However, because the complex processes affecting movement of water at the very low concentrations present in the Bandelier Tuff are not entirely resolved, the Area G model assumes a steady-state vertical flux of liquid water.

Assuming a steady-state 5 mm/yr in the Area G simulation, the groundwater travel time through about 100 m of Bandelier Tuff is 600 years. Taking into account the data in Table 2 comparing the hydrology of Area G and the Los Alamos County landfill, the groundwater travel time through the Bandelier Tuff beneath the Los Alamos County landfill is expected to exceed 1,200 years. The groundwater travel time is the *minimum* time required for radionuclides to be transported through the Bandelier Tuff. Most of the radionuclides will be retarded by physico-chemical interactions with minerals in the tuff, resulting in much longer transport times.

Table 3 shows the effective sorption coefficients, which indicate the degree to which elements are retarded within the Bandelier Tuff. Applying these numbers to radioisotopes of a given element to the nominal 1,200-year groundwater travel time, the time required for various radioisotopes to be transported through the Bandelier Tuff beneath the Los Alamos County landfill is estimated. The long transport times indicate that a large quantity of radioactivity could be safely disposed of at the Los Alamos County landfill without contaminating the regional aquifer. Many of the radioisotopes identified previously in Table 1 will decay into stable elements before they are transported through the vadose zone. The table excludes those radionuclides listed previously in Table 1 that will decay to stable elements within 1,200 years (i.e., $\tau_{1/2} < 120$ years).

Table 3. Sorption coefficients for long-lived radionuclides in the *Green is Clean* inventory

Radionuclide	Sorption Coefficient (mL/g)[15]	Transport Time (yrs)[16]
Al-26	1.3E+02	1.4E+06
Si-32	3.5E+01	3.9E+05
Cl-36	0.0E+00	1.2E+03
Ca-41	1.2E+02	1.3E+06
Ni-59, 63	5.0E+01	5.5E+05
Nb-91, 91m, 92, 93, 94, 95	1.0E+02	1.1E+06
Mo-93	4.0E+00	4.4E+04
Tc-95m, 97, 98, 99	0.0E+00	1.2E+03
La-137	1.0E+02	1.1E+06
Gd-148, 150	5.0E+01	5.5E+05
Tb-157, 158	1.0E+00	1.1E+06
Pt-193	5.0E+01	5.5E+05
Pb-202, 205	2.5E+01	2.8E+05
Bi-207, 208	2.0E+00	1.1E+04
Po-209	2.0E+00	1.1E+04
U-234, 235, 238	2.4E+00	2.6E+04
Np-237	2.3E+00	2.5E+04
Pu-238, 239, 240, 241, 242	4.1E+00	4.5E+04
Am-241, 243	2.4E+03	2.6E+07

3. MODELING RESULTS

The results of the dose assessment and groundwater-protection analysis provide the technical basis for establishing radionuclide thresholds that *Green is Clean* waste verification instruments must be capable of detecting. The most restrictive analysis, that is, the analysis resulting in the lowest threshold, is proposed as the required detection limit. The public dose and groundwater-protection constraints are both met by the thresholds established in the much more restrictive worker and future resident scenarios.

The 1-mrem thresholds calculated for a wide variety of radionuclides present in radiological areas at LANL using the methodology summarized in Section 2 are provided in Table 4. The values listed are mass concentrations for individual radionuclides that, alone, result in a 1-mrem dose to a worker or to a future resident according to the scenarios described in Section 2. Threshold values take into account that the anticipated volume of *Green is Clean* waste (500 cubic meters) is a small fraction of the total volume of waste disposed of in the county landfill (150,000 cubic meters)[2]. The 1-mrem threshold values calculated for a number of the radionuclides exceed the natural specific activities. In this case, the specific activity of the radionuclide was chosen as the future resident-based limit.

The threshold limits that will be the qualifying basis for *Green is Clean* verification instruments will be the minimum of the two calculated values. The radionuclide thresholds for slightly more than half of the isotopes included in the analysis are based on projected exposures to the disposal facility worker. These radionuclides typically have half-lives of a few days or years, high specific activity, and relatively large external dose conversion factors. By the end of the 30-year institutional control period, when exposures to the future resident were first postulated to occur, the short-lived isotopes will have decayed significantly. The future resident limits for the long-lived transuranics are relatively low due to their relatively large 50-year dose conversion factors.

Many of the radionuclides in the table undergo radioactive decay, forming one or more decay products. The limits for these radionuclides are based on the assumption that only the parent radionuclide is present at the time the waste is generated. Ingrowth of daughter products begins at the time of waste generation and continues through the end of the 1,000-year dose assessment period.

The radionuclide threshold mass-concentrations listed in Table 4 apply when the each individual radioisotope is the only potential contaminant in the waste. To determine the 1-mrem threshold for waste potentially containing a mixture of radionuclides, it is necessary to use the "sum of fractions" rule. Under this rule, the minimum detectable activity for each radionuclide potentially present in the waste must be divided by the applicable threshold limit. The sum of fractions for all radionuclides in the waste must be less than unity to ensure that the instrument may be used to verify that waste. This rule also applies to situations when daughter products are present at the time of assay.

Table 4. 1-mrem thresholds for *Green is Clean* waste verification

Radionuclide	Worker Dose Threshold (pCi/g)	Resident Dose Threshold (pCi/g)	Limiting Threshold (pCi/g)	Limiting Scenario
Be-7	4.0E+03	3.5E+17(a)	4.0E+03	Worker
Na-22	8.2E+01	1.4E+05	8.2E+01	Worker
Al-26	6.8E+01	4.2E+01	4.2E+01	Resident
Si-32	9.8E+05	7.9E+02	7.9E+02	Resident
Ti-44	1.0E+02	9.2E+01	9.2E+01	Resident
V-48	6.3E+01	1.7E+17(a)	6.3E+01	Worker
V-49	2.3E+08	8.1E+15(a)	2.3E+08	Worker
Cr-51	8.0E+03	9.2E+16(a)	8.0E+03	Worker
Mn-54	2.5E+02	1.1E+13	2.5E+02	Worker
Co-56	5.6E+01	3.0E+16(a)	5.6E+01	Worker
Co-57	4.2E+03	3.8E+15	4.2E+03	Worker
Co-58	2.1E+02	3.2E+16(a)	2.1E+02	Worker
Fe-59	1.6E+02	4.9E+16(a)	1.6E+02	Worker
Ni-59	6.1E+07	1.7E+06	1.7E+06	Resident
Co-60	7.6E+01	2.5E+03	7.6E+01	Worker
Ni-63	2.3E+07	7.8E+05	7.8E+05	Resident
Zn-65	3.7E+02	5.6E+15	3.7E+02	Worker
Ge-68	2.2E+02	1.3E+14	2.2E+02	Worker
As-73	2.0E+07	2.2E+16(a)	2.0E+07	Worker
As-74	2.7E+02	9.9E+16(a)	2.7E+02	Worker
Se-75	6.2E+02	1.4E+16(a)	6.2E+02	Worker
Sr-82	1.9E+02	6.4E+16(a)	1.9E+02	Worker
Rb-83	4.3E+02	1.9E+16(a)	4.3E+02	Worker
Rb-84	2.4E+02	4.7E+16(a)	2.4E+02	Worker
Sr-85	4.2E+02	2.4E+16(a)	4.2E+02	Worker
Rb-86	2.2E+03	8.1E+16(a)	2.2E+03	Worker
Zr-88	2.5E+02	1.7E+16(a)	2.5E+02	Worker
Nb-91	1.3E+05	7.6E+04	7.6E+04	Resident
Nb-91m	5.5E+03	2.2E+16(a)	5.5E+03	Worker
Nb-92	1.2E+02	7.3E+01	7.3E+01	Resident
Nb-93	---(b)	---(b)	---(b)	---(b)
Nb-94	1.2E+02	7.4E+01	7.4E+01	Resident
Nb-95	2.5E+02	3.9E+16(a)	2.5E+02	Worker

Tc-95m	1.5E+02	2.3E+16(a)	1.5E+02	Worker
Zr-95	2.3E+02	2.1E+16(a)	2.3E+02	Worker
Tc-97	1.5E+05	3.9E+04	3.9E+04	Resident
Tc-97m	1.1E+07	4.1E+11	1.1E+07	Worker
Tc-98	1.4E+02	8.1E+01	8.1E+01	Resident
Tc-99	9.3E+06	8.7E+03	8.7E+03	Resident
Rh-101	5.2E+06	2.0E+08	5.2E+06	Worker
Rh-102	1.4E+06	6.8E+07	1.4E+06	Worker
Rh-102m	3.4E+06	2.8E+08	3.4E+06	Worker
Ag-108m	1.2E+02	8.6E+01	8.6E+01	Resident
Cd-109	1.0E+06	1.9E+11	1.0E+06	Worker
Ag-110m	7.3E+01	3.7E+14	7.3E+01	Worker
Cd-113m	8.0E+04	3.8E+03	3.8E+03	Resident
Sn-113	8.3E+02	1.0E+16(a)	8.3E+02	Worker
La-137	1.9E+07	4.5E+06	4.5E+06	Resident
Eu-150	1.7E+06	8.5E+05	8.5E+05	Resident
Gd-150	---(b)	---(b)	---(b)	---(b)
Eu-152	1.8E+02	5.7E+02	1.8E+02	Worker
Dy-154	---(b)	---(b)	---(b)	---(b)
Eu-154	1.5E+02	3.4E+02	1.5E+02	Worker
Tb-157	2.1E+05	1.3E+05	1.3E+05	Resident
Tb-158	2.6E+06	6.8E+05	6.8E+05	Resident
Hf-172	1.3E+06	2.4E+10	1.3E+06	Worker
Lu-173	1.2E+07	1.3E+13	1.2E+07	Worker
Lu-174	1.1E+07	9.7E+08	1.1E+07	Worker
Lu-174m	6.6E+06	8.1E+09	6.6E+06	Worker
Hf-178m	4.7E+05	3.6E+05	3.6E+05	Resident
Ta-179	4.6E+07	1.4E+12	4.6E+07	Worker
Ta-182	1.8E+02	6.2E+15(a)	1.8E+02	Worker
Re-183	4.5E+03	1.0E+16(a)	4.5E+03	Worker
Re-184	2.3E+02	1.9E+16(a)	2.3E+02	Worker
Re-184m	3.1E+02	4.2E+15(a)	3.1E+02	Worker
Os-185	3.3E+02	7.5E+15(a)	3.3E+02	Worker
Hg-194	2.0E+02	1.3E+02	1.3E+02	Resident
Pb-202	5.9E+02	3.3E+02	3.3E+02	Resident
Bi-207	1.3E+02	1.6E+02	1.3E+02	Worker
Bi-208	6.3E+01	4.2E+01	4.2E+01	Resident
Po-209	6.8E+04	4.9E+04	4.9E+04	Resident
U-234	1.77E+04	2.5E+03	2.5E+03	Resident
U-235	1.62E+03	6.3E+02	6.3E+02	Resident
Np-237	7.80E+02	2.0E+02	2.0E+02	Resident
Pu-238	2.33E+03	1.3E+03	1.3E+03	Resident
U-238	7.02E+03	2.6E+03	2.6E+03	Resident
Pu-239	2.07E+03	9.3E+02	9.3E+02	Resident
Pu-240	2.07E+03	9.3E+02	9.3E+02	Resident
Am-241	1.90E+03	3.0E+04	1.9E+03	Worker
Pu-241	8.46E+04	8.4E+02	8.4E+02	Resident
Pu-242	2.18E+03	9.7E+02	9.7E+02	Resident
Am-243	9.14E+02	4.5E+02	4.5E+02	Resident

[a]. Radionuclide concentration limit is set equal to the radionuclide's specific activity.

[b]. Concentration limit could not be calculated as dose conversion factors were unavailable.

4. DISCUSSION

The proposed detection thresholds presented in Table 4 were developed to ensure that no harm to human health would occur, should radioactivity be inadvertently present but undetected in *Green is Clean* waste that is free-released to the Los Alamos County landfill. The actual detection limits of the systems proposed for verifying *Green is Clean* waste were developed independent of the dose assessment thresholds. Detailed technical reports describing the systems are available.[17,18] The detection limits reported in those reports are compared with the proposed detection thresholds in Table 5.

Table 5. Instrument detection limits compared with 1-mrem thresholds.

Radionuclide	Instrument Detection Limit (pCi/g)	1-mrem Threshold Concentration (pCi/g)
Be-7	3.2E+01	4.0E+03
Na-22	1.2E+00	8.2E+01
Al-26	1.3E+00	4.2E+01
Ti-44	7.0E-01	9.2E+01
V-48	1.1E+00	6.3E+01
Cr-51	3.4E+01	8.0E+03
Mn-54	3.4E+00	2.5E+02
Fe-55	1.6E+00	2.1E+07
Co-56	1.1E+00	5.6E+01
Co-57	3.5E+00	4.2E+03
Co-58	3.3E+00	2.1E+02
Fe-59	3.2E+00	1.6E+02
Co-60	1.7E+00	7.6E+01
Zn-65	6.3E+00	3.7E+02
Ge-68	1.9E+00	2.2E+02
As-73	3.2E+01	2.0E+07
As-74	2.5E+00	2.7E+02
Se-75	1.9E+00	6.2E+02
Sr-82	9.5E-01	1.9E+02
Rb-83	3.6E+00	4.3E+02
Rb-84	2.8E+00	2.4E+02
Sr-85	3.4E+00	4.2E+02
Rb-86	3.8E+01	2.2E+03
Zr-88	1.1E+00	2.5E+02
Sr-90	3.6E-01	9.1E+02
Nb-92	1.7E+00	7.3E+01
Nb-94	1.7E+00	7.4E+01
Nb-95	3.4E+00	2.5E+02
Tc-95m	2.2E+00	1.5E+02
Zr-95	1.5E+00	2.3E+02
Tc-97	1.4E-07	3.9E+04
Tc-97m	1.1E+03	1.1E+07
Tc-98	1.7E+00	8.1E+01
Tc-99	2.2E-06	8.7E+03
Rh-101	2.1E+00	5.2E+06
Rh-102	1.0E+00	1.4E+06
Rh-102m	3.0E+00	3.4E+06
Ag-108m	9.7E-01	8.6E+01

Cd-109	9.4E+01	1.0E+06
Ag-110m	1.0E+00	7.3E+01
Cd-113m	1.5E+02	3.8E+03
Sn-113	5.1E+00	8.3E+02
La-137	4.5E+00	4.5E+06
Pm-145	4.1E+00	3.2E+04
Eu-150	9.3E-01	8.5E+05
Eu-152	1.4E+00	1.8E+02
Eu-154	1.7E+00	1.5E+02
Tb-157	1.7E+01	1.3E+05
Tb-158	1.8E+00	6.8E+05
Hf-172	6.8E-01	1.3E+06
Lu-173	3.1E+00	1.2E+07
Lu-174	3.6E+00	1.1E+07
Lu-174m	1.9E+00	6.6E+06
Hf-178m	2.3E+00	3.6E+05
Ta-179	7.2E+00	4.6E+07
Ta-182	1.5E+00	1.8E+02
Re-183	2.0E+00	4.5E+03
Re-184	1.7E+00	2.3E+02
Re-184m	1.0E+00	3.1E+02
Os-185	1.9E+00	3.3E+02
Hg-194	1.6E+00	1.3E+02
Pb-202	1.9E+00	3.3E+02
Bi-207	3.2E+01	1.3E+02
Bi-208	2.5E+00	4.2E+01
Po-209	4.3E+02	4.9E+04
U-234	8.2E-01	2.5E+03
U-235	1.2E-01	6.3E+02
Np-237	8.8E-02	2.0E+02
Pu-238	8.2E-01	1.3E+03
U-238	2.0E-01	2.6E+03
Pu-239	1.9E+00	9.3E+02
Pu-240	1.9E+00	9.3E+02
Am-241	1.1E-01	1.9E+03
Pu-241	5.7E+00	8.4E+02
Pu-242	1.0E+00	9.7E+02
Am-243	3.0E-01	4.5E+02

Table 6 compares these calculated thresholds with exempt concentrations found in the *State of New Mexico Radiation Protection Regulations*.[19] The table includes only those radionuclides that are both 1) listed in the regulations and 2) identified as being present in LANL radiological controlled areas; the exempt mass concentration is, in many cases, larger than the proposed detection threshold. The fourth column of Table 6 lists the detection threshold to which the *Green is Clean* waste verification systems have been qualified.

Table 6. Comparison of calculated thresholds and NMED exempt concentrations

Radionuclide	Exempt Concentration (pCi/g)	1-mrem Threshold Concentration (pCi/g)	Detection Threshold (pCi/g)
Be-7	2.0E+04	4.0E+03	3.2E+01
V-48	3.0E+02	6.3E+01	1.1E+00
Cr-51	2.0E+04	8.0E+03	3.4E+01
Mn-54	1.0E+03	2.5E+02	3.4E+00
Fe-55	8.0E+03	2.1E+07	1.6E+00
Co-56	1.00E+00	5.6E+01	1.1E+00
Co-57	5.0E+03	4.2E+03	3.5E+00
Co-58	1.0E+03	2.1E+02	3.3E+00
Fe-59	6.0E+02	1.6E+02	3.2E+00
Co-60	5.0E+02	7.6E+01	1.7E+00
Zn-65	1.0E+03	3.7E+02	6.3E+00
Ge-68	1.0E+00	2.2E+02	1.9E+00
As-73	5.0E+03	2.0E+07	3.2E+01
As-74	5.0E+02	2.7E+02	2.5E+00
Se-75	3.0E+03	6.2E+02	1.9E+00
Sr-82	1.0E+00	1.9E+02	9.5E-01
Rb-83	1.0E+00	4.3E+02	3.6E+00
Rb-84	1.0E+00	2.4E+02	2.8E+00
Sr-85	1.0E+00	4.2E+02	1.7E+00
Rb-86	7.0E+02	2.2E+03	3.4E+00
Zr-88	1.0E+00	2.5E+02	1.1E+00
Nb-94	1.2E+02	7.4E+01	1.7E+00
Nb-95	1.0E+03	2.5E+02	3.4E+00
Tc-95m	1.0E+00	1.5E+02	2.2E+00
Zr-95	6.0E+02	2.3E+02	1.5E+00
Rh-101	1.0E+00	5.2E+06	2.1E+00
Rh-102	1.0E+00	1.4E+06	1.0E+00
Rh-102m	1.0E+00	3.4E+06	3.0E+00
Cd-109	2.0E+03	1.0E+06	9.4E+01
Ag-110m	3.0E+02	7.3E+01	1.0E+00
Sn-113	9.0E+02	8.3E+02	5.1E+00
Pm-145	1.0E+00	3.2E+04	4.1E+00
Eu-150	1.0E+00	8.5E+05	9.3E-01
Eu-152	6.0E+02	1.8E+02	1.4E+00
Lu-173	1.0E+00	1.2E+07	3.1E+00
Lu-174	1.0E+00	1.1E+07	3.6E+00
Lu-174m	1.0E+00	6.6E+06	1.9E+00
Hf-178m	1.0E+00	3.6E+05	2.3E+00
Ta-179	1.0E+00	4.6E+07	7.2E+00
Ta-182	4.0E+02	1.8E+02	1.5E+00
Re-183	6.0E+03	4.5E+03	2.0E+00
Re-184	1.0E+00	2.3E+02	1.7E+00
Re-184m	1.0E+00	3.1E+02	1.0E+00
Os-185	7.0E+02	3.3E+02	1.9E+00
Hg-194	1.0E+00	1.3E+02	1.6E+00

5. CONCLUSIONS

The information summarized in this report and detailed in references cited herein provide a high degree of confidence in the ability of the LANL to ensure that disposal of *Green is Clean* waste at the Los Alamos County landfill will not pose a threat to human health or the environment. The initial *Green is Clean* waste segregation activities performed and documented by waste generators and the verification of segregated *Green is Clean* waste before release to the County landfill provide defense in depth: Should the segregation step fail, the verification step ensures that waste containing potentially harmful amounts of radioactivity will not be released. The detection thresholds calculated in the dose assessment ensure that instruments used to verify *Green is Clean* waste are capable of detecting radioactivity in amounts that would result in a 1-mrem dose, which is 0.3 percent of the natural background radioactivity in the Los Alamos region. The detection protocols developed by the *Green is Clean* waste generating organizations provide an additional level of assurance, being capable of detecting, in most cases, orders of magnitude below the 1-mrem thresholds determined in the dose assessment.

6.0 REFERENCES

[1] U.S. DOE (1995), "Response to Questions and Clarification of Requirements and Processes: DOE 5400.5, Section II.5, and Chapter IV (Requirements Relating to Residual Radioactive Material," U.S. DOE Office of Environmental Management, November 17, 1995

[2] Personal communication between D. Hollis, LANL and R. Stafford, NMED, September 24, 1996

[3] Shuman, R.(1996), "Radionuclide Concentration Limits for the Disposal of Waste with Low Levels of Radioactivity at the Los Alamos County Landfill," Rogers and Associates Engineering Corp., RAE-9148/84-1

[4] Personal communication between D. Hollis, LANL, and V. Valdez, L.A. County, July 17, 1996

[5] Hollis, D. et al. (1997), "Performance Assessment and Composite Analysis for LANL MDA G," LA-UR-97-85

[6] Personal communication between D. Hollis, LANL, and Phil Weston, NMED, July 17, 1996

[7] Vold, E. L. and R. Shuman (1997), "A Model for the Biotic Translocation of Buried Low-Level Radioactive Waste to the Ground Surface in the Presence of Surface Erosion," LA-UR-97-84

[8] CAP-88

[9] Vold, E. L. (1996a), "Atmospheric Transport in Complex Terrain at Los Alamos, Area G," LA-UR-96-4870

[10] Kennedy, W.E. and R.A. Peloquin (1988) "Intruder Scenarios for Site-Specific Low-Level Radioactive Waste Classification," DOE/LLW-71T

[11] Newell, D. (1997), "Justification for Scaling the TA-54, Area G Performance Assessment Transport Model to the Los Alamos County Landfill," Internal EM-SWO Memorandum, July 28, 1997

[12] Newman, B. D. (1996), "Vadose Zone Water Movement at Area G, Los Alamos National Laboratory, TA-54: Interpretations Based on Chloride and Stable Isotope Profiles," LA-UR-96-4682

[13] Vold, E.L. (1996b), "Analysis of Liquid Phase Transport in the Unsaturated Zone at a Mesa Top Disposal Facility," LA-UR-96-320

[14] Vold, E.L. (1996c), "An Analysis of Vapor Phase Transport in the Unsaturated Zone with Application to a Mesa Top Disposal Facility, Part I," LA-UR-96-973

[15] Longmire, P. (1997) Personal Communication between P. Longmire, LANL CST-7 and D. Hollis, LANL EM-SWO, August 5, 1997

[16] Birdsell, K. et al. (1995) "Numerical Modeling of Unsaturated Groundwater Flow and Radionuclide Transport at MDA G," LA-UR-95-2735

[17] Dry, D. et al. (1997), "Analysis of TA-48 Waste Boxes," Draft CST-11 Report

[18] Myers, S. (1997), "Technical Evaluation of the WAND System," BEC Report R-1006 for EM-SWO

[19] "State of New Mexico Radiation Protection Regulations," Environment Department, Radiation Licensing and Registration Section," Santa Fe, NM 87502-6110, May 3, 1995

APPENDIX B

BASIC PROPERTIES OF THE POISSON STATISTICAL DISTRIBUTION

The Poisson statistical distribution is given by

$$P(n,\bar{n}) = \frac{(\bar{n})^n \, e^{-\bar{n}}}{n!} \quad ,$$

where the function gives the probability of observing n occurrences of an event when the average number observed is $\bar{n}$.

As required for a normalized distribution

$$\sum_{n=0}^{\infty} P(n,\bar{n}) = 1 \quad .$$

The first moment of the distribution is given by

$$\sum_{n=0}^{\infty} nP(n,\bar{n}) = \bar{n} \quad .$$

The second moment with respect to the mean is given by

$$\sum_{n=0}^{\infty} (n-\bar{n})^2 P(n,\bar{n}) = \bar{n} \quad ,$$

which by definition means that Variance $= \sigma^2 = \bar{n}$ and, of course, that Standard Deviation $= \sigma = \sqrt{\bar{n}}$.

The next four relations are useful in computing actual values of the distribution when n and/or $\bar{n}$ are large, in that one avoids computing exponentials and factorials for large numbers, which can easily exceed the capabilities of small computers.

Trivially, of course,

$$P(0,\bar{n}) = e^{-\bar{n}} \quad ,$$

but it is very useful in connection with the upward and downward recursion relations:

$$P(n+1,\bar{n}) = \left(\frac{\bar{n}}{n+1} \right) P(n,\bar{n}) \quad ,$$

and

$$P(n-1,\bar{n}) = \left(\frac{n}{\bar{n}}\right) P(n,\bar{n}) \quad .$$

Stirling's approximation, which is sometimes useful for large values of n and/or $\bar{n}$, is given by:

$$P(n,\bar{n}) \cong \frac{1}{\sqrt{2\pi n}} \left(\frac{\bar{n}}{n}\right)^n e^{-(\bar{n}-n)} \quad .$$

For $n = 10$ its error is about 0.8%, for $n = 100$ its error is 0.08%, and the error is less for larger values of n. It is worth noticing that if $\bar{n}$ is an integer,

$$P(\bar{n}-1,\bar{n}) = P(\bar{n},\bar{n}) \quad .$$

Finally, in order to demonstrate the asymmetry of the Poisson distribution for small $\bar{n}$ we give Fig. B-1, for $\bar{n} = 2.5$. For values of $\bar{n}$ greater than about 20, the Poisson distribution is so nearly equal to the familiar Normal distribution—which is in general easier to manipulate—that the Normal is nearly always used.

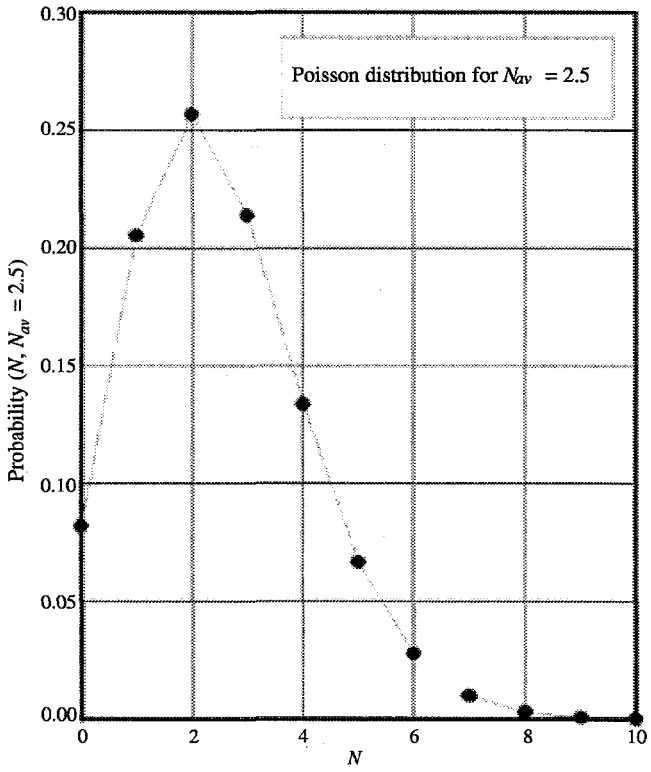

Fig. B-1. The Poisson probability distribution for an average count of 2.5, indicating the basic assymetric nature of the distributions for small values of the average count. For average values of about 20 and greater, the Poisson distribution is very nearly equal to the familiar, symmetric normal distribution.